Laser Assisted Cold Spray of Aluminum Alloy 6061

A Thesis Presented

By

Samuel Mason Boese

to

The Department of Mechanical & Industrial Engineering

in partial fulfillment of the requirements
for the degree of

Master of Science
in the field of
Mechanical Engineering

Northeastern University
Boston, Massachusetts

August 2024

Abstract

Cold spray (CS) is an additive manufacturing technology used in applications including repair and 3D printing. CS can create deposits using high feed rates while minimizing oxidation, porosity, and residual stress. Traditionally, CS has been performed with helium as the carrier gas, but the increasing cost of helium makes it a less viable solution. The process can also be done with nitrogen gas, but the resulting deposit has inferior mechanical properties when compared to deposits made with helium. Laser assisted cold spray (LACS) can be used to enhance the properties of CS deposits created using nitrogen gas. In this work, aluminum alloy 6061 (Al6061) was deposited with CS using nitrogen gas at laser powers up to 6 kW. The laser was aimed coincident with the spray spot and the temperature was monitored with a pyrometer. The heat added at the spray spot by the laser allows increased material deformation resulting in improved bonding between deposited particles, otherwise known as splats. As a result, the strength of the deposits increased from 34.3 MPa to 167.6 MPa, and elongation increased from 0.07% to 15.58%, when comparing the 0 kW and 5 kW cases, respectively. X-ray diffraction (XRD) revealed that using laser heating during deposition increases residual stress in the deposit, but its effects can be counteracted by using a hotplate beneath the substrate. Fatigue testing showed that fatigue performance was largely driven by tensile strength, and the 3 kW and 5 kW samples performed similarly. Adhesion strength was tested for various laser powers. By increasing the laser power from 1 kW to 6 kW, adhesion strength was increased from 18.4 MPa to 76.8 MPa. Metallurgical analysis revealed that heat added by the laser leads to precipitation

growth, reduced hardness, recrystallization, and improved bonding between splats. These metallurgical changes significantly improved the bulk mechanical properties of the deposits. LACS may have similar success with other aluminum alloys, or materials that are typically difficult to deposit, such as refractory metals.

Acknowledgements

I would like to thank Professor Müftü for advising this work. His involvement and assistance went above and beyond what was expected, and his support brought this project to its highest potential. I would also like to thank Dr. Ozan Özdemir for his assistance on this project. He was the source of a few key technical recommendations that allowed the ideas in this study to be a success. I would also like to thank Dr. Ahmad Nourian-Avval for his contributions. His knowledge in the field of material science was heavily relied upon. I learned a lot from him, and our discussions played a significant role in developing my interest in material science.

I would like to thank my colleagues in the cold spray lab. Tricia Schwartz taught me nearly everything I know about operating and managing a research lab. Much of my knowledge about project execution, equipment operation, and time management comes from her. A special thanks goes out to Aidan Sevinsky. A significant portion of the analysis in this work was completed with his help. His positive attitude and excitement for material science motivates everyone in the lab and I am happy to have him as a colleague. Thank you to my other co-workers Jon Gager, Kevin McCarthy and all the co-op students who helped us along the way. This project would not have come to fruition without all of you.

Table of Contents

List of Tables

List of Figures

1 Introduction

1.1 Background

Cold spray (CS) is a line-of-sight solid-state additive manufacturing process used to deposit powder particles onto a substrate. This technique involves injecting powder particles, typically metals, into a high-pressure heated gas stream that flows through a converging-diverging de Laval nozzle, accelerating the particles to supersonic speeds. When particles impact the substrate or previously deposited layers, they undergo severe plastic deformation, resulting in a combination of metallurgical bonding and mechanical interlocking [1]. The deposited powder particles are called splats. Unlike high-temperature processes, such as laser cladding and thermal spray, which induce oxidation, phase transformation, and substantial residual stress [2], CS avoids these issues by not exceeding the material's melting point. Therefore, the relatively low temperatures of CS makes it suitable for repair of components [3], deposition of corrosion and wear-resistant coatings [4, 5], and additive manufacturing of near net shape parts [6].

Al6061 is one of the most common aluminum alloys and is used across many industries including defense, automobile, marine, and aerospace. It has relatively high strength, exhibiting an ultimate tensile strength (UTS) of 310 MPa. It also has corrosion resistance and good machinability [7]. Many Al6061 components are used in dynamic applications that induce wear over time, therefore, methods of repairing such components with CS is needed. Further, 3D printing Al6061 components with CS instead of using subtractive manufacturing methods could lead to improved lead times and decreased cost [1].

1.2 Motivation

In this study, LACS with nitrogen gas is used to deposit Al6061 powder on Al6061-T6 substrate by using laser emission powers ranging between 0-6 kW to expand our knowledge base in understanding the benefits LACS can provide for improving mechanical performance of cold spray deposits. To this end, achievable tensile strength, ductility, residual stress, fatigue performance, and adhesion strength of LACS deposits were characterized as a function of laser power. Metallographic analysis of these specimens was performed to seek correlations between the microstructural changes and the bulk deposit properties. The outcomes are discussed within the context of traditional Al6061 heat treatments.

2 Literature Review

2.1 Cold Spray

Considerable research effort has been dedicated to optimizing the spray conditions and evaluating the mechanical properties of Al6061 cold sprayed with helium [7-14]. Work has been completed to understand the bonding mechanism between particles. Analysis shows the formation of metallurgical bonds between splats, accompanied with extensive recrystallization near the interfacial regions [9]. Tailoring the feedstock in order to achieve changes in properties such as homogenous grain structures has been investigated [10, 11]. Property improvement with end application in mind has also been done, including increasing wear resistance and minimizing porosity [7]. Improvements in mechanical properties have been made with post-deposition heat treatments [8]. Fatigue properties have been tested along with the effects of surface finish and heat treatment [12, 13]. Fracture toughness has also been thoroughly tested at different orientations in order to quantify the degree of anisotropy with the deposits [14].

Limited research has been conducted to CS deposition of this alloy using nitrogen gas [15-18]. The mechanical properties of Al6061 cold sprayed with nitrogen fall short of wrought Al6061 or Al6061 cold sprayed with helium [14, 19]. Particles sprayed in helium achieve greater impact velocities than in nitrogen, due to the differing expansion properties of each gas [20]. Currently, helium is about thirty times more expensive than nitrogen. Therefore, a solution to spraying Al6061 in nitrogen must be found [21]. One strategy is to use homogenized powder to improve spray quality [17]. Homogenized powder has high ductility and therefore can deform more easily upon impact, leading to stronger inter-splat bonding. Other research has shown that post-spray treatments can improve the deposit's properties, including thermal [5, 13, 16], or thermo-mechanical [3, 22] treatments. Studies

have explored the benefit of in-situ micro-forging, in which a hard powder material, such as stainless steel, is mixed with a soft powder material, such as aluminum. The hard powder provides additional compression on the soft powder during deposition, which enhances the inter-particle bonding and improves the mechanical properties [16]. These methods are effective in increasing the mechanical properties compared to as-sprayed CS deposits, but require an additional powder mixing, powder-treatment or post-treatment step.

2.2   Laser Assisted Cold Spray

Laser-assisted cold spray (LACS) is a single-step approach for increasing the strength and ductility of cold spray deposits using nitrogen. LACS involves in-situ heating of the substrate or pre-deposited material by a laser, reducing the critical velocity of the particles, and enhancing the inter-particle bonding at velocity levels provided by nitrogen gas. LACS could be useful in applications where applying post-spray heat treatment is challenging, such as the repair of large components or the production of components composed of dissimilar materials. LACS has been used for various deposition of materials, including 4340 steel [23], Ni and Al [24], Fe-Ni-Zr [25], Ti-6Al-4V [26], Cu [27], and Al – 12wt% Si [28]. These works demonstrated that LACS can improve the deposition efficiency (DE) and reduce the porosity level in CS deposits. The DE in these deposits is improved due to the thermal softening provided by laser heating, which in turn results in more plastic deformation during deposition and improved inter-splat bonding. However, the aforementioned studies stop short of testing the mechanical properties of the deposits, and addressing the challenges that arise from depositing thick coatings at high laser powers. These challenges include heat accumulation, residual stress buildup, delamination, and

substrate warping. Fewer studies have been done examining the mechanical properties of LACS deposits. Significant improvement in the adhesion strength of copper deposited on steel using LACS has been reported by optimizing laser parameters such as spot size and laser power. Pull off tests showed that ideal conditions increased the adhesion strength from 13 MPa to 82 MPa[29]. LACS has also been used to improve the adhesion of Al6061. However, relatively low laser powers were used (~1 kW), and the improvements were limited, showing a bond strength improvement from 27 MPa and 48 MPa [30]. The work in this thesis aims to use higher laser powers, up to 6 kW, and perform extensive mechanical and metallurgical testing in order to improve Al6061 CS deposits.

3 Materials & Methods

3.1 LACS setup and sample preparation

The experimental setup shown in Figure 1 consists of a VRC Gen III (Elsworth, SD, USA)

CS system equipped with a YLS-6000-CUT-Y17 laser system manufactured by IPG

Photonics® (Oxford, MA, USA). An Impac IGA 140 pyrometer made by Advanced

Energy® (Denver, CO, USA), is used to measure the surface temperature at the deposition

site. Air knives are used to protect the laser's cover-glass from rebounding particles. The

CS gas stream and the laser beam are focused on the same spot on the substrate, and the

pyrometer measures the temperature of the center of this area. The laser has a collimated

continuous beam with a 10 mm diameter.
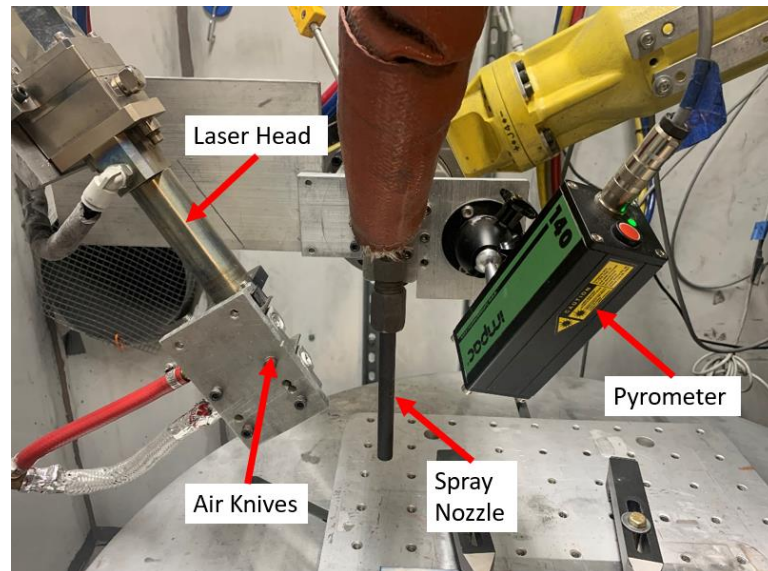
Figure 1. Experimental setup of the LACS system.

Feedstock Al6061 powder (SAAM-Al6061-G1H1, Solvus Global®, Worcester, MA,

USA), was sprayed onto Al6061-T6 substrate (McMaster-Carr®, Elmhurst, IL) using the

process parameters given in Table 1.

Table 1. CS parameters used in this study.

Parameter	Value
Gas Pressure (MPa)	6.55
Gas Temperature (°C)	425
Powder Feeder Gas Flow (SLM)	125
Powder Feed Rate (g/min)	5.5
Nozzle Orientation (°)	90
Nozzle Traverse Speed (mm/s)	200
Nozzle Material	Polybenzimidazole (PBI)
Nozzle Model	VRC® NZZL0070
Nozzle Throat Diameter (mm)	2
Nozzle Exit Diameter (mm)	6.3
Nozzle Length (mm)	170
Nozzle Standoff (mm)	40
Pre-heat layer	Single pass without powder feed

The primary goal of this study was to optimize the mechanical performance of Al6061 deposits including tensile strength, ductility, fatigue performance, and adhesion strength. To achieve this, four groups of specimens, shown in Table 2, were sprayed and tested. In Group 1, tensile specimens were sprayed to examine changes in strength and ductility at different laser powers. Different heating and insulating conditions at the bottom of the substrate were explored to see how changing the thermal boundary condition would affect the microstructure and mechanical performance. In Group 2, specimens were sprayed to analyze residual stresses within the deposits. Residual stress in cold sprayed deposits can lead to delamination, and often need to be minimized. Therefore, the effect of the laser on residual stress was studied. Fatigue testing was performed by using the parameters in Group 3 to determine performance at high laser powers. High laser powers were chosen because they showed high strength in the Group 1 tensile testing results. In Group 4, bond buttons were sprayed to characterize the deposit's adhesion strength at different laser powers. These groups and their naming conventions are summarized in Table 2. The first

two letters indicate the sample geometry (TS=tensile, RS=residual stress, F=fatigue, and BB=bond button), the following number indicates the laser power in kW, and the last letter indicates the condition at the bottom of the substrate (T=table, I=insulation, and H=hotplate).

Table 2. Designation of different groups and performed tests.

Group 1: Tensile		Group 2: Residual Stress	
Sample ID	Performed Tests	Sample ID	Performed Tests
TS-0kW-T TS-0kW-I TS-0kW-H TS-1kW-H TS-3kW-H TS-5kW-H	Tensile / Fractography Porosity Micro-hardness Nano-hardness Microstructural characterization (SEM, TEM, EBSD)	RS-0kW-T RS-0.5kW-T RS-0.5kW-H	Residual Stress
Group 3: Fatigue		**Group 4: Bond Buttons**	
Sample ID	Performed Tests	Sample ID	Performed Tests
F-3kW-H F-5kW-H	Fatigue / Fractography	BB-1kW-T BB-2.5kW-T BB-4kW-T BB-5kW-T BB-6kW-T	Adhesion

3.2 Mechanical and microstructural characterization

To test the tensile properties of the deposits, blocks of material were first sprayed at different laser powers then machined into tensile test specimens according to ASTM E8 [31]. The test conditions are summarized in Group 1 of Table 2. The substrates were Al6061-T6 plates with dimensions 100 mm x 150 mm x 12.5 mm. A shallow channel was milled at the bottom of each substrate to insert a thermocouple. The substrates were prepared by abrading the surface with 3M Scotchbrite™ and cleaning with ethanol. The robot raster was programmed for a length of 200 mm, width of 50 mm and thickness of 35 layers, resulting in a deposit height of approximately 6.25 mm. To reduce high-temperature

gradients at the interfacial region between the spray and substrate, the substrates were each heated with the spray jet and laser without feeding powder for one layer, referred to here as a preheat layer. The preheat layer was performed prior to each deposition.

Deposits were performed with laser powers of 0 kW, 1 kW, 3 kW, and 5 kW. For the 1 kW, 3 kW, and 5 kW cases, delamination occurred during deposition. To resolve this issue, heat was applied to the bottom of the substrate by using a hotplate (IKA® Works Inc., C-MAG HP 7, Wilmington, NC). The hotplate was set to its maximum temperature, 500°C, which provided a temperature of 330°C at the substrate surface. Samples were also made at 0 kW with the hotplate, and 0 kW with insulation. The insulation was 12.5 mm thick calcium silicate (McMaster-Carr®, Elmhurst, IL) cut to match the size of the substrate. The insulation was added to test if retaining heat in the system during the spray would lead to improved mechanical properties and was applied between the substrate and build plate.

The deposits were machined into sub-size tensile specimens in accordance with ASTM E8 [31]. Sub-size specimens were chosen to reduce the material cost. The machined specimens had a 25.4 mm gauge length and a 6.35 mm x 3.18 mm cross section. For each condition in Group 1 of Table 2, two blocks were sprayed, and three tensile specimens were machined out of each block, yielding a total of six tensile tests for each condition, for total of 36 samples. Tensile testing was completed on a 100 kN AGS-X Universal Electromechanical Test Frame made by Shimadzu® (Kyoto, Japan). Strain was recorded using an Epsilon 3542-0100-050-ST contact extensometer made by Epsilon Technology Corp.® (Jackson, WY, USA). High magnification images of the fracture surfaces were taken with a Thermo Fisher Scientific Inc.® (Waltham, MA, USA) Scios Dualbeam scanning electron microscope (SEM). The images were taken at 2,500x magnification and 5 kV beam power.

Polished metallographic samples were prepared from the leftover material in the tensile block. Cross sections were made perpendicular to the robot traverse direction. Samples were ground down to 1,200 grit and polished using 1 μm polycrystalline diamond suspension then finished with 0.05 μm colloidal silica. Images for porosity measurements were taken for all samples using a Zeiss Axioscope® 7 MAT (Oberkochen, Germany). The ZEN CORE (Zeiss, Oberkochen, Germany) image analysis software was used to measure the porosity. Four porosity measurements at 200x magnification were taken for each sample at random locations.

Vickers microhardness was measured using an ALPHA MHT-2000 semi-automatic tester made by Pace Technologies® (Tucson, AZ, USA). Indents were made in a plane perpendicular to the substrate-deposit interface (i.e. through thickness direction) with a load of 200 g and a dwell time of 15 s. Two profiles were made per sample.

The polished cross sections were etched with Keller's reagent then SEM imaging was performed to visualize the splats. Images were taken at 5,000x and 8,000x magnification and 5 kV beam power. An open-source analysis software, ImageJ (NIH, USA), was used to measure the percentage of the splat interface that is bonded to the surrounding splats. A bonding ratio was calculated based on these measurements [19]. The percentage reported for each specimen group is an average of four measurements.

Transition electron microscopy (TEM) was performed to study splat interfaces by using a Titan Themis 300 S/TEM made by Thermo Fisher Scientific Inc.® (Waltham, MA, USA). Samples were prepared by using focused ion beam (FIB) milling. This was performed at the polar region of a splat. This allows analysis of the interface between splats. The TEM images were taken at 15,500x magnification. Energy-dispersive X-ray spectroscopy (EDS)

was performed during TEM analysis using SuperX EDS made by Thermo Fisher Scientific Inc.® (Waltham, MA, USA). Electron backscatter diffraction (EBSD) images were taken with a Hikari EBSD detector and OIM Analysis 8 software made by EDAX® (Mahwah, NJ, USA). Analysis was done at 15 kV with a 100 nm step size with 1,500x magnification.

To analyze the residual stress state, deposits with the conditions in Group 2 (Table 2) were prepared. The substrates were 50 mm x 75 mm x 6.13 mm, and the spray dimensions were 25 mm x 50 mm x 6.13 mm. Residual stress was examined under three conditions: (1) no laser, (2) laser, and (3) laser and hotplate. A laser power of 500 W was chosen so that the deposit remained laminated to the substrate in all three conditions. The hotplate was set to 200°C. The remainder of the spray conditions are given in Table 1. One deposit was prepared for each condition, for a total of three deposits.

The samples were sectioned along the raster direction, as shown in Figure 2. The samples were electropolished to remove any stresses induced during sectioning. Measurements were taken with X-ray diffraction (XRD) using a XStress DR45 made by Stresstech Ltd.® (Vaajakoski, Finland). The tube power was 30 kV x 9 mA, the collimator diameter was 0.3 mm, and the exposure time was 15 s. The nominal locations for measurements were through the coating height at 0.76, 1.52, 2.29 and 3.05 mm with the origin being the substate-coating interface.
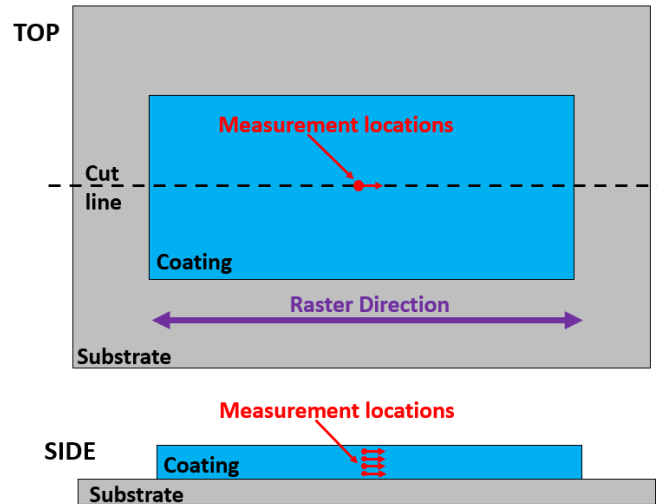
Figure 2 Locations and direction of residual stress measurements on CS sample.

For fatigue testing, two laser power levels were used (Group 3, Table 2). Blocks were deposited using the same procedure as the tensile specimens. Fatigue samples were made using laser powers of 3 kW and 5 kW with the hotplate set to 500°C. The laser power of 3 kW was used because the tensile results showed a significant increase in strength, while 5 kW was selected because its tensile results showed a significant increase in ductility. Specimens were manufactured in accordance with ASTM E466 [32]. Eight specimens were manufactured for each condition, for a total of 16 samples. Specimens were tested with a stress ratio of -1 and 15 Hz at various stress amplitude levels with runout set at 5×10^6 cycles.

The adhesion strength of the CS deposits were evaluated by preparing bond button specimens according to ASTM C633 [33]. These evaluations were performed on cylindrical Al6061-T6 specimens, coated with Al6061 powders using different levels of laser power, including 1 kW, 2.5 kW, 4 kW, 5 kW, and 6 kW. In each case, six layers were coated, which yielded a thickness of 0.6 mm. Before coating, the cylindrical specimens' surfaces were abraded with 3M Scotchbrite™ and cleaned with ethanol.

The coated bond buttons were glued to non-sprayed bond buttons using FM® 1000 epoxy (Cytec Industries®, Princeton, NJ, USA) and cured at 176°C for 2 hours. The assembled bond buttons were then pulled until failure, using a 100 kN AGS-X Universal Electromechanical Test Frame made by Shimadzu® (Kyoto, Japan). For each experimental group, six adhesion specimens and one control specimen were prepared and tested, yielding a total of 35 specimens in Group 4 of Table 2. The control specimen is two non-sprayed bond buttons epoxied together to verify the epoxy strength.

4 Results & Discussion

4.1 Changes in microstructure due to the laser

For the different spray conditions in Group 1 (Table 2), temperature data was collected at the spray spot and at the bottom of the substrate. The spray spot temperature was recorded using the pyrometer and the substrate bottom temperature was recorded using a thermocouple. This data was averaged for the entirety of each spray condition and is given in Table 3.

Table 3. Average spray spot and substrate bottom temperatures for different spray conditions.

Sample	Spray Spot T (°C)	Substrate Bottom T (°C)
TS-0kW-T	180 ± 4.6	119 ± 3.9
TS-0kW-I	192 ± 4.2	141 ± 5.1
TS-0kW-H	203 ± 9.5	177 ± 4.2
TS-1kW-H	250 ± 12.1	196 ± 3.6
TS-3kW-H	350 ± 12.6	229 ± 4.5
TS-5kW-H	455 ± 13.7	257 ± 8.4

For Al6061, there are critical heat treatment temperatures that are useful in predicting the effects of the laser. Artificial aging of Al6061 to create a T6 temper is typically done at 160°C for 18 hours or 170°C for 8 hours. These temperatures allow controlled precipitation growth that results in a strengthened material. Above the recommended artificial aging range (150°C - 200°C) the material can be overaged. Overaging causes precipitates to grow to the point of becoming incoherent with the material around them, and allow dislocations to move more freely, resulting in a soft temper. The higher the temperature, the shorter period of time it takes to overage the material [34]. Based on the spray spot and thermocouple readings, it can be expected that artificial aging, and potentially overaging, will occur for samples made with the laser (TS-1kW-H, TS-3kW-H, and TS-5kW-H).

Annealing of Al6061 is typically done at 415°C for 2-3 hours. At this temperature, high diffusion rates are achieved, resulting in large precipitates, and minimum hardness. The annealing temperature is surpassed at the spray spot for sample TS-5kW-H, implying that significant softening is occurring during deposition.

EDS was used to identify the size and distribution of precipitates near the splat interface. EDS results are shown in Figure 3. The distribution of Mg is shown alongside the scanning transition electron microscopy (STEM) images. Si is not shown because it coexisted with Mg, potentially in the form of Mg_2Si, which is a primary precipitate in Al6061 [34]. In the TS-0kW-T sample, the precipitates are small and ordered linearly along the grain boundaries. This cellular precipitate structure inhibits dislocation movement, which can cause brittleness. As more heat is added in the TS-0kW-H and TS-3kW-H cases, the precipitates begin to conglomerate into larger structures. In the TS-5kW-H case, precipitation has evolved into large, round, isolated structures, typical of overaged and annealed Al6061 [34]. This structure is a result of the high temperature at the spray spot, ~455°C, achieved by 5 kW of laser power. At this temperature, diffusion rates are high, and precipitates can grow in relatively short timeframes. Large precipitation allows dislocations to move freely through the matrix, resulting in lower hardness and higher ductility.
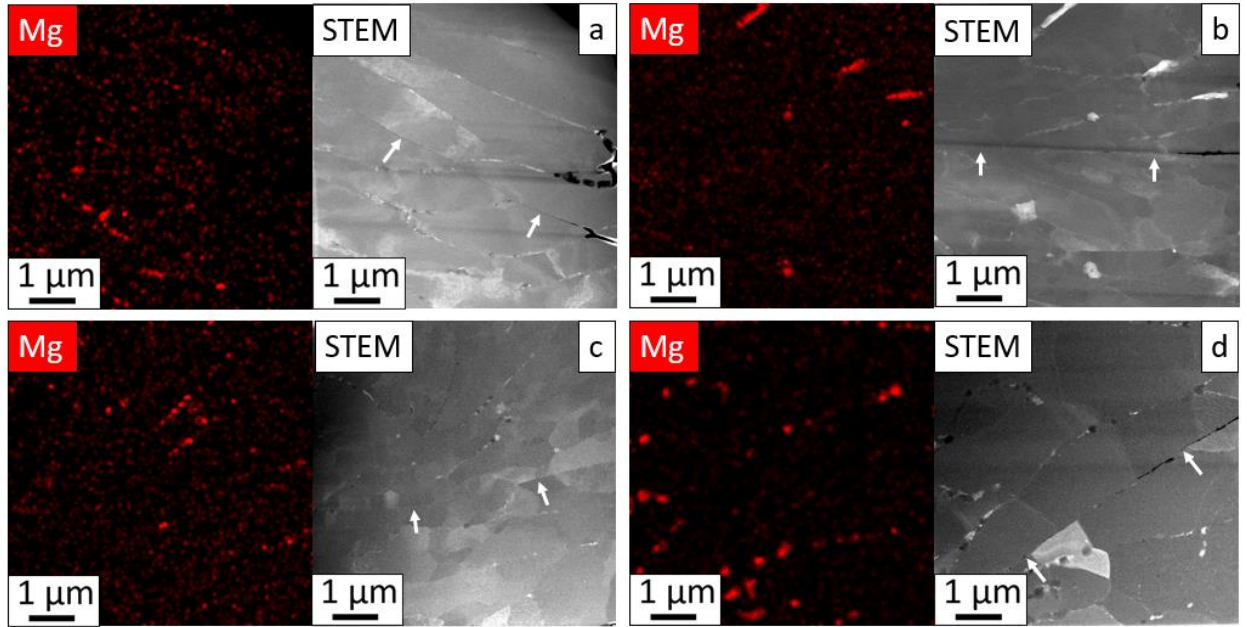
Figure 3. EDS images of Mg and correlating STEM images for (a) TS-0kW-T, (b) TS-0kW-H, (c) TS-3kW-H, and (d) TS-5kW-H. The splat interface is identified with white arrows.

The interface between splats was further examined using TEM in order to observe dislocation density and grain structure. TEM images are shown in Figure 4. The TS-0kW-T case in Figure 4a shows non-uniform diffraction patterns resulting in cloudiness, caused by elastic distortion of the crystal lattice, which is an indication of stress within the grains. The distortion of the lattice is due to deformation that occurred during deposition when the powder particle made impact. The addition of heat from the hotplate (TS-0kW-H) allows increased mobilization of dislocations, resulting in some recrystallization. This process leads to distinct grain structures with lower dislocation densities as indicated by a decrease in cloudiness, as seen in Figure 4b. This effect is present in the TS-3kW-H case shown in Figure 4c and is most prominent for the TS-5kW-H case shown in Figure 4d. It is known that as heat input increases, so does the mobility of grain boundaries and dislocations, resulting in recrystallization [34]. For TS-5kW-H, the grains near splat interface are large,

equiaxed, and have low dislocation density. The decrease in dislocation density reduces the possibility of dislocation entanglement, which in turn decreases the hardness and increases the ductility. The large equiaxed grains with low internal stress allow the migration of dislocations when exposed to stress, which could result in ductile bulk material behavior.
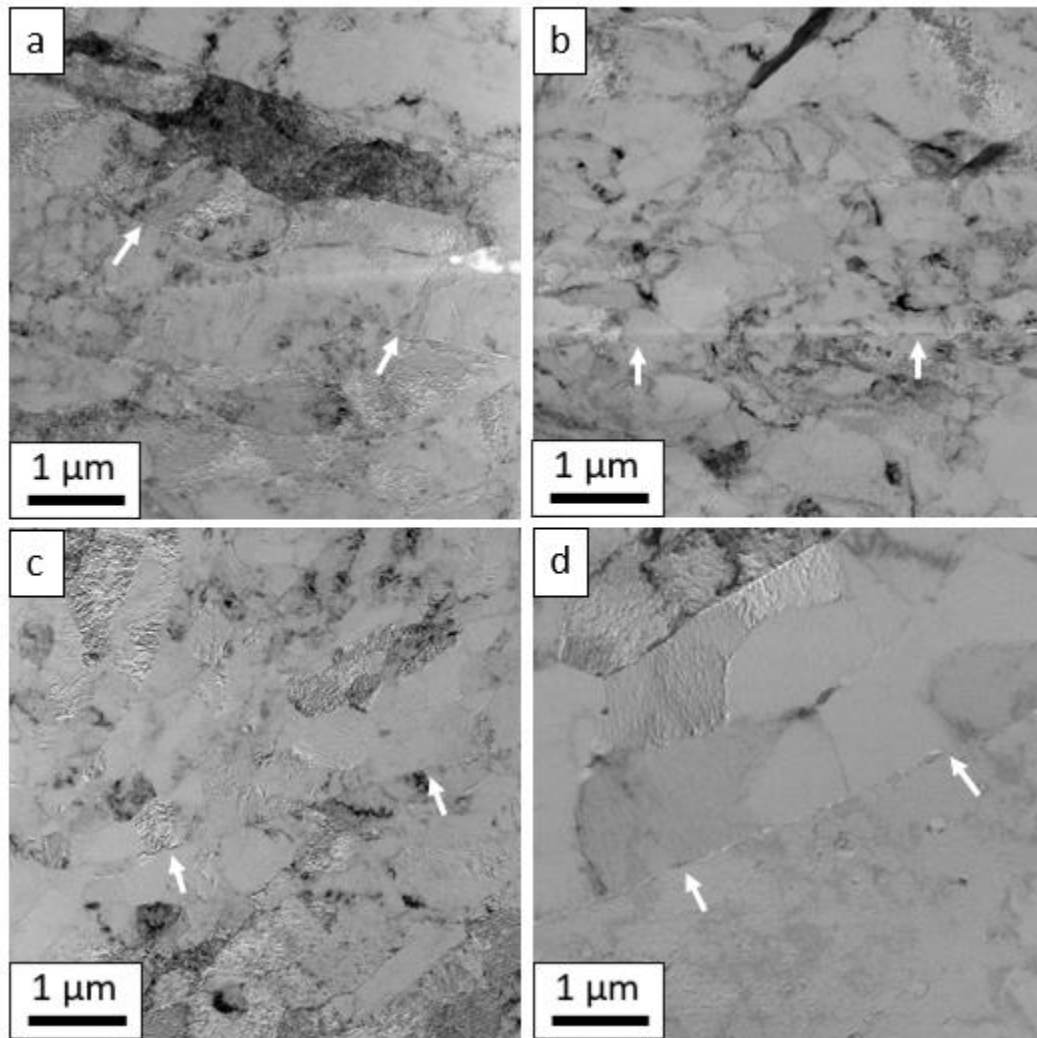

Figure 4. TEM images for (a) TS-0kW-T, (b) TS-0kW-H, (c) TS-3kW-H, and (d) TS-5kW-H. The interface is identified with white arrows.

EBSD was performed on the sample cross sections in order to compare grain size and shape. The inverse pole figures (IPFs) obtained from EBSD are shown in Figure 5. The

TS-0kW-T case shows significant grain refinement at the splat interfaces. This is likely caused by dynamic recrystallization in response to severe plastic deformation during particle impact. The high strain rates experienced during deposition are resolved through the formation of ultra-fine grains (UFGs) near the splat interfaces. The grains further within the splats are deformed, showing a flattened structure due to impact. As more heat is added by the hotplate and laser, recrystallization and grain coarsening allow the splats to form equiaxed grains. The UFGs around the splat boundaries experience grain growth, resulting in a more uniform grain structure. This effect is limited in the TS-0kW-H and TS-1kW-H cases but is more prominent in the TS-5kW-H case. This agrees with the TEM results in Figure 4d which show recrystallized grains near the interface for sample TS-5kW-H. In general, aluminum alloys achieve sufficient grain boundary mobility needed for recrystallization at temperatures >250°C [34]. Based on the temperature data in Table 3, the TS-5kW-H deposit is likely held above 250°C for the duration of deposition, allowing a significant amount of recrystallization to occur.
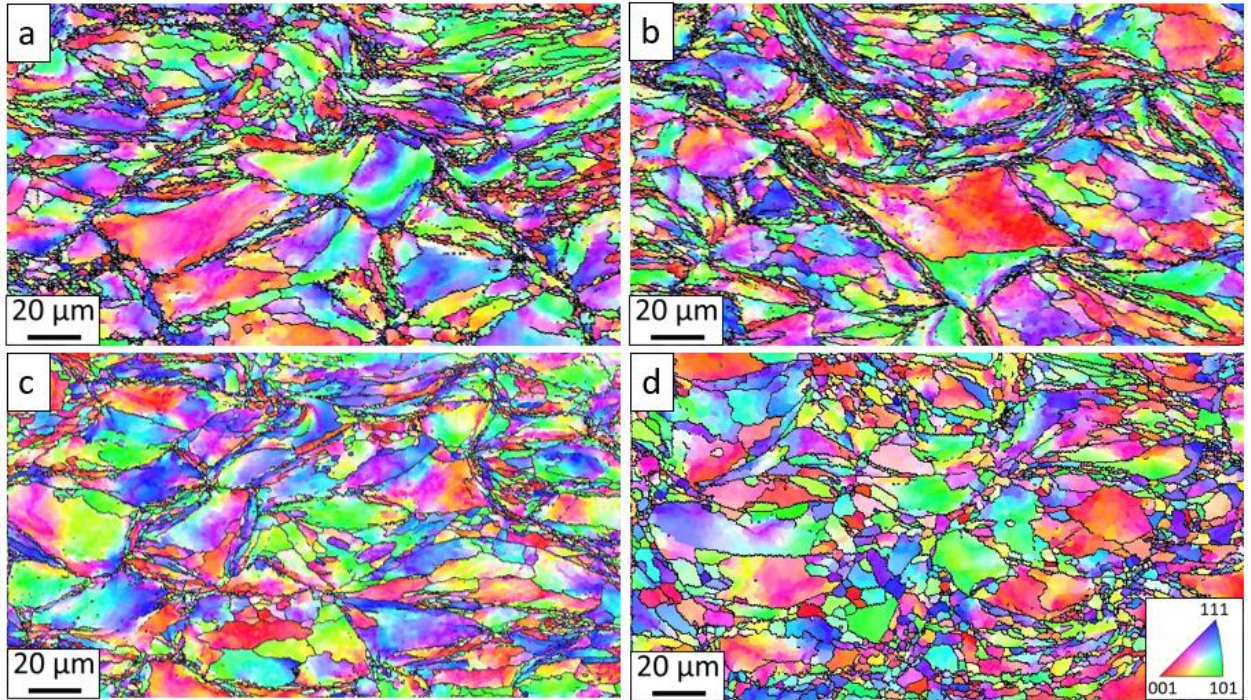
Figure 5. IPFs for (a) TS-0kW-T, (b) TS-0kW-H, (c) TS-1kW-H, and (d) TS-5kW-H.

Nanoindentation was performed on the polished cross sections using a NanoTest Vantage system made by Micro Materials® (Wrexham, UK) fitted with a Berkovich pyramid indenter. Indents were made in a 10x10 grid using a 3 mN load and 10 μm spacing. Hardness contours overlayed with SEM images are shown in Figure 6. Chemical etching was performed after hardness testing to minimize error in the hardness measurements caused by uneven surfaces and surface chemistry changes. The TS-3kW-H case leads to a decrease in average hardness from 1.44 GPa to 1.12 GPa. The TS-5kW-H case leads to a further decrease in hardness to 0.86 GPa and increased uniformity throughout the measurement area, as the standard deviation decreases from 0.16 GPa in the control case to 0.05 GPa in the 5 kW case. This data aligns with the EDS and TEM data shown in Figure 3 and Figure 4, respectively. As precipitation size increases and dislocation density decreases, dislocations are able to move unobstructed, resulting in a softer material. These

changes happened because TS-3kW-H and TS-5kW-H were held above the artificial aging
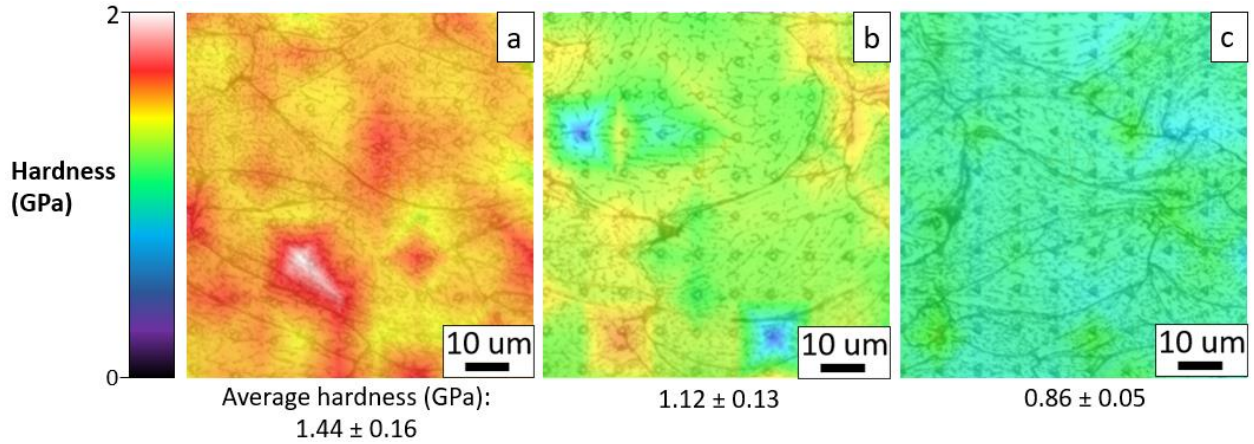
temperature range and were therefore overaged.

Figure 6. Nanoindentation results for (a) TS-0kW-T, (b) TS-3kW-H, and (c) TS-5kW-H.

Micro-hardness data is plotted in Figure 7. The horizontal axis shows the indent location,

where zero is the interface, positive values are the spray deposit, and negative values are

the substrate. The measured hardness value for wrought Al6061-T6 was 106 ± 2 HV and

is indicated in Figure 7 by a green dashed line. The control case (TS-0kW-T) has a substrate

hardness similar to the measured hardness of Al6061-T6 and a deposit hardness in the

range of 80-90 HV. The absence of substrate softening for the TS-0kW-T case implies that

regular CS does not modify the substrate properties substantially. When the hotplate is

involved in the spray without the laser (TS-0kW-H), we find that the substrate softens from

100 HV to 50 HV because the heat from the hotplate overages the substrate. We also see

that the deposit softens slightly from 80 HV to 70 HV. A similar result is obtained when

LACS is used with 3 kW of laser power (TS-3kW-H). However, when the laser power is

increased to 5 kW (TS-5kW-H), the deposit hardness is further reduced to approximately

50 HV. This change can be tied to the metallurgical results, where 5 kW causes substantial

precipitation growth, recrystallization and grain coarsening, due to high heat input. In summary, using the hotplate to heat the substrate results in reducing the hardness of the substrate, whereas high laser power reduces the hardness of the deposited layers.
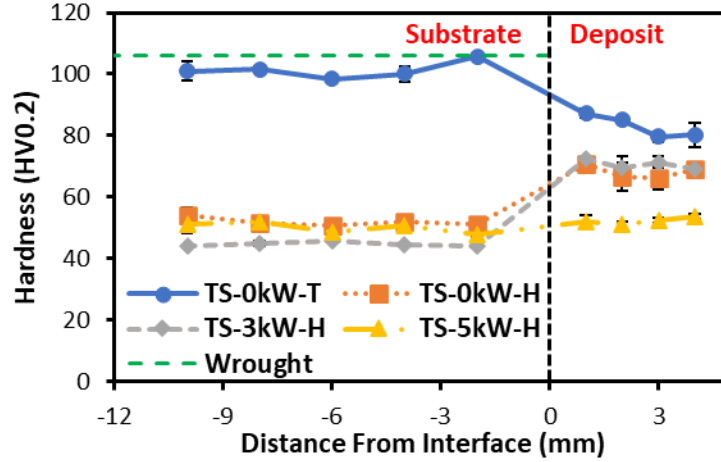

Figure 7. Hardness profiles for various samples. Positive distance is the CS deposit and negative distance is the substrate.

4.2 Material softening due to the laser

The in-situ softening effect of the laser can be estimated using the Johnson-Cook model, given below.

$$\sigma_y = \left(A + B\varepsilon_p^n\right)(1 + Cln\dot{\varepsilon})(1 - T^{*m}) \tag{1}$$

The equation estimates the effects of equivalent plastic strain (ε_p), strain rate ($\dot{\varepsilon}$), and homologous temperature (T^*) on the yield stress (σ_y). The material constants for Al6061, A, B, C, n and m, are taken from the literature to be 270, 154.3, 0.002, 0.239 and 1.42, respectively [35]. For deposited splats being impacted by incoming particles, the strain rate is taken to be 10^8 s^{-1} [36]. The equivalent plastic strain would be varying throughout the impact. The homologous temperature can be calculated from temperature (T) using Eq. (2), where T_{ref} is room temperature (25°C) and T_m is the melting point (585°C).

$$T^* = (T - T_{ref})/(T_m - T_{ref}) \tag{2}$$

Based on the pyrometer measurements summarized in Table 3, yield strength of the splats can be calculated across different values of ε_p. The results are plotted in Figure 8. It is seen that at each temperature, an increase in ε_p leads to an increase in σ_y due to strain hardening. However, temperature seems to play a more dominant role in determining σ_y for higher laser powers. Significant loss of strength is seen at 350°C, which correlates to sample TS-3kW-H. This decrease is even more significant at 455°C, which correlates to sample TS-5kW-H. Therefore, it can be concluded that an increase in temperature caused by the laser leads to a drastic decrease in yield strength, allowing splats to deform more easily during impact. Deformation causes a breakdown of the oxide layer on the outside of a powder particle, and leads to closer contact between splats, which could improve the bonding between splats.
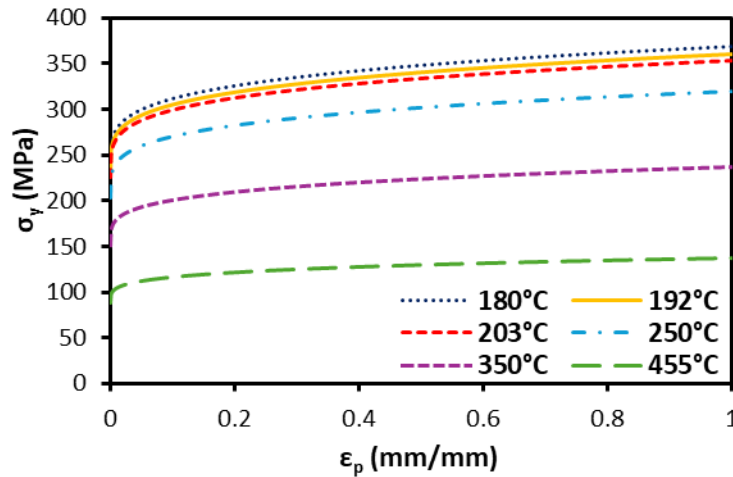

Figure 8. Yield stress versus equivalent plastic strain for different temperatures. Strain rate is 10^8 s^{-1} to represent a particle impact.

4.3 Porosity and bonding ratio

Average porosity values for Group 1 are shown in Figure 9a. The data shows that increasing the laser power from 0 kW to 3 kW decreases the porosity from 1.73% to 0.73%. Increasing the laser power to 5 kW causes a further decrease in porosity to 0.24%. The increase in laser power increases the temperature at the deposition spot, which decreases the yield strength and allows the splats to deform more, thus closing the pores. Additionally, material diffusion due to heat input reduces porosity. High heat leads to diffusion across the splat interfaces, which can close small pores and cracks within the deposit. It has been noted in the literature that heat treatment can "heal" defects in cold spray deposits [37, 38]. It is likely that the in-situ laser treatment causes healing similar to a post-spray heat treatment, and also plays a role in reducing porosity.

In order to determine the quality of bonding between splats, polished samples were etched then examined using SEM. Some of these images are presented in Figure 10. The percentage of the interface that is bonded to the surrounding splats is called the bonding ratio [19]. The bonding ratio is determined by dividing the total length of a splat interface by the summation of the portions that are well bonded. Average bonding ratios are plotted in Figure 9b. The values are an average of four measurements taken on four different splats for each sample. In the case of TS-0kW-T, the interface around the splat is poorly bonded, with an average bonding ratio of 3.7%. With the addition of the hotplate in TS-0kW-H, the interface is still poorly bonded to the surrounding splats. With the addition of laser power, in TS-3kW-H, there are portions of the splat that are well bonded. When laser power is increased to 5kW, in sample TS-5kW-H, the amount of well bonded interfaces increases even more than the 3kW case, resulting in an average of 35.5% bonding. The increase in

bonding ratio is likely due to a combination of material behaviors. The high heat input from the laser decreases the yield strength of the splats before they are impacted by incoming particles. The decrease in yield strength allows closer contact between splats, which is a requirement for bond formation. Secondly, the laser and hotplate cause the entire deposit to remain at an elevated temperature throughout deposition. The overall increase in temperature can cause unbonded splat boundaries to heal and form bonds due to diffusion across splat boundaries. An increase in bonding ratio could lead to an increase in strength and ductility in the bulk deposit because it is the bonds between splats that hold the deposit together.
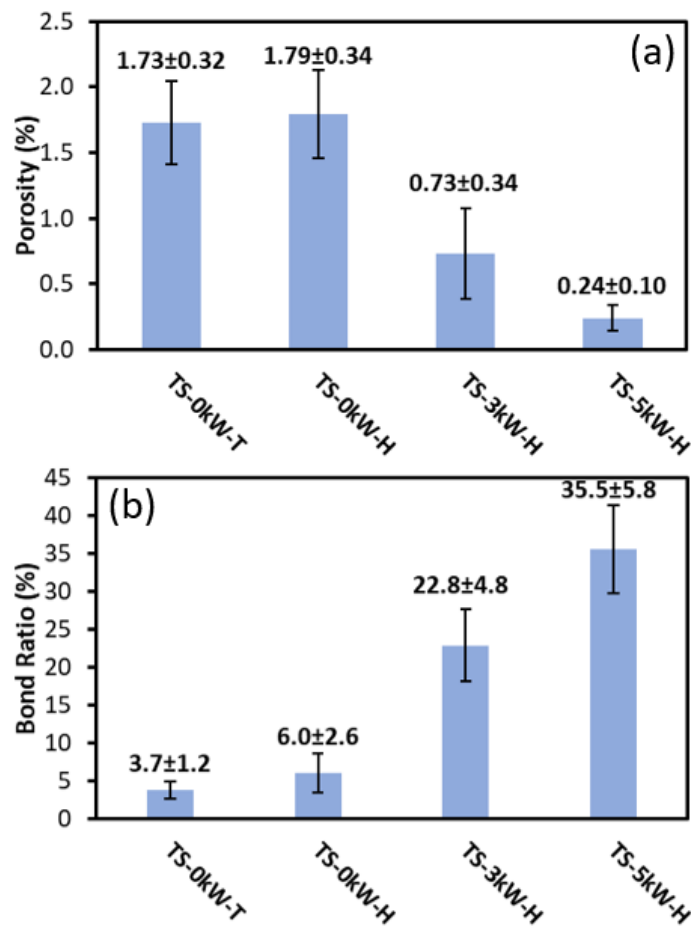

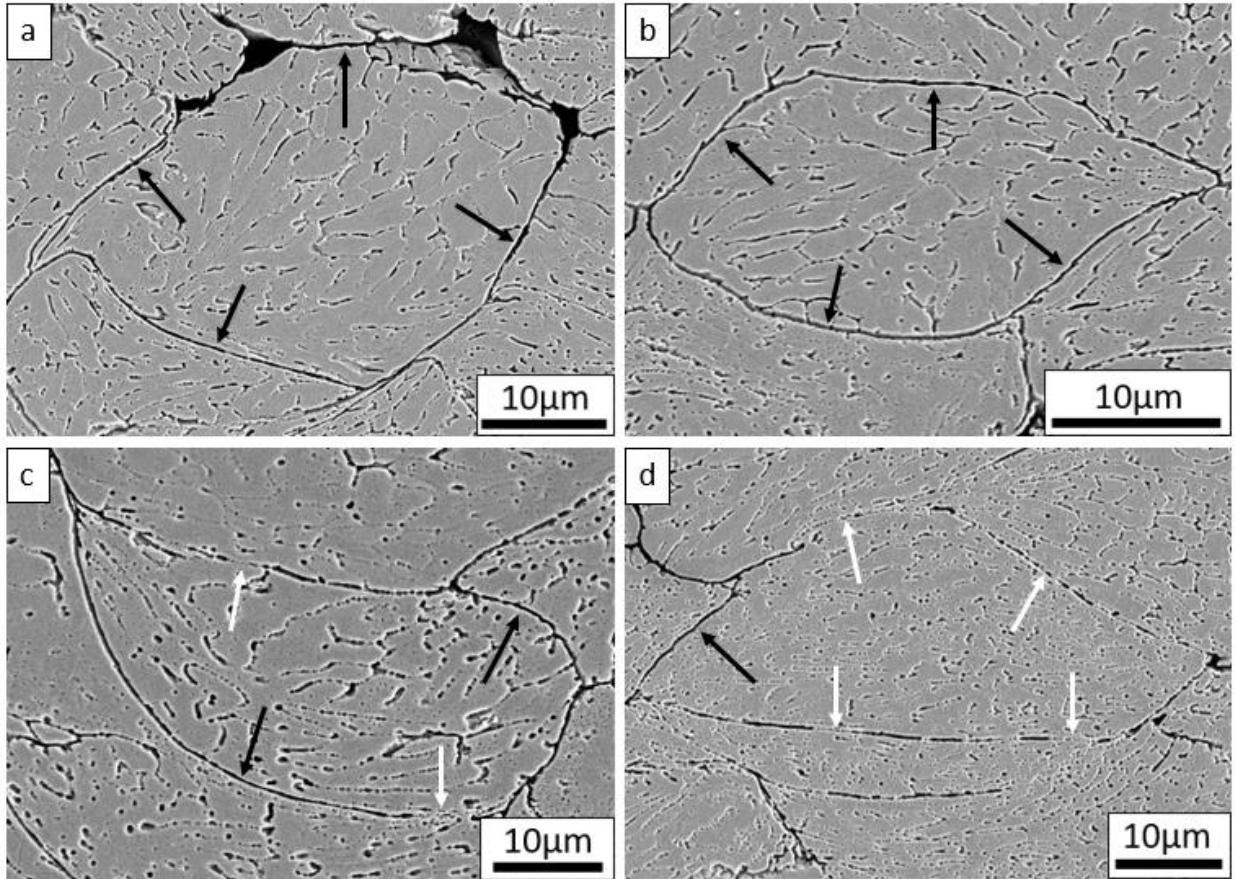Figure 9. (a) Porosity and (b) bonding ratio for Al6061 LACS deposits.

Figure 10. SEM of etched deposits. Images are of samples (a) TS-0kW-T, (b) TS-0kW-H, (c) TS-3kW-H, and (d) TS-5kW-H. Poorly bonded regions are indicated with black arrows and well bonded regions are indicated with white arrows.

4.4 Tensile results and fractography

The stress-strain curves of samples with significant differences in tensile properties are compared in Figure 11. There is a significant increase in strength from 34 MPa for the sample deposited with no laser and without using the hotplate (TS-0kW-T) to 165 MPa for the sample deposited with 3 kW of laser power while using the hotplate (TS-3kW-H). The hotplate is set to its max temperature, 500°C, in all cases where it is used, providing a surface temperature of 330°C. When the laser power is increased to 5 kW (TS-5kW-H), there is a drastic increase in ductility to 15.6% without decreasing the strength.
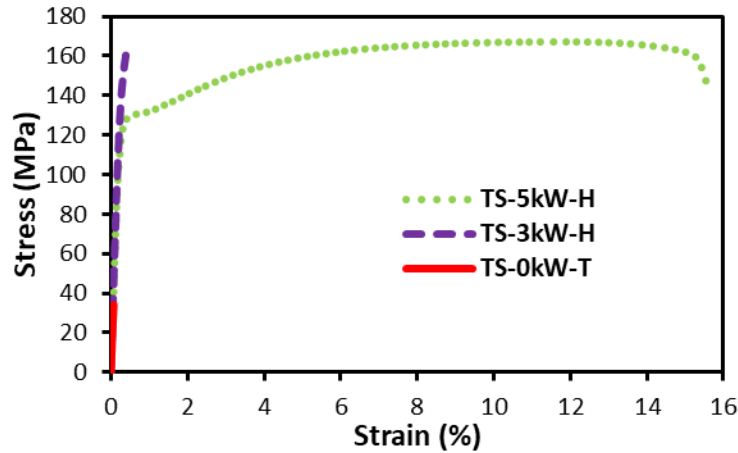
Figure 11. Stress-strain curves for different deposition conditions.

Ultimate tensile stress (UTS) and percent elongation at fracture (%EL) were obtained from the tensile tests and summarized in Figure 12. The temperature of the spray spot recorded by the pyrometer is given on the top abscissa. The deposition conditions for each sample set are indicated on the bottom abscissa. Six samples were tested for each condition. The UTS of wrought Al6061-T6 and cold spray deposited using helium gas are taken from the literature [14]. The samples mounted directly to the table without any external heating or insulation (TS-0kW-T) fail at 34.3 MPa, which is approximately 10% of the strength of wrought Al6061-T6. The heat added to the system by the hotplate (TS-0kW-H), or heat retained in the system by the insulation (TS-0kW-I) have noticeable effects on the UTS, presumably because the previously deposited layers are softened by the added or retained heat, allowing improved inter-splat bonding. However, the most significant improvements are seen with the addition of laser power. By using 5 kW of laser power (TS-5kW-H), the strength is increased to 167.6 MPa, which is approximately 50% the strength of wrought Al6061-T6.
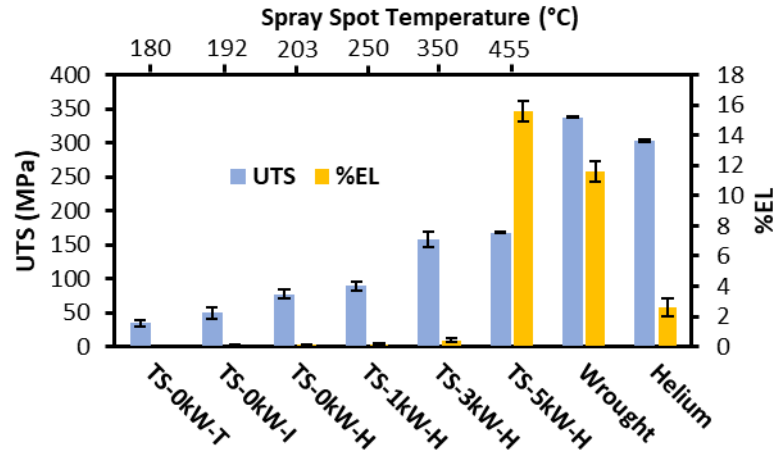
Figure 12. UTS, %EL, and spray spot temperature for different deposition conditions.

Slight improvements in ductility can be achieved by the addition of the hotplate, insulation, or the use of the laser up to 3 kW. It is interesting to note that laser power levels of 1 kW and 3 kW result in modest values of %EL. However, at 5 kW of laser power, there is a drastic increase in ductility. The elongation of the tensile samples is found to be 15.58% for the cases where a hotplate is used to keep the substrate temperature high and the laser power is set to 5 kW (TS-5kW-H). It should be noted that this level of ductility is greater than the ductility of deposits made with helium (2.6% [14]) and wrought Al6061-T6 (11.6% [14]) but less than the annealed condition, Al6061-O (25-30% [34]).

Temperature readings from the pyrometer are shown on the top abscissa of Figure 12. Insulating or putting a hotplate under the substrate increases the temperature at the spray spot. As the laser power increases, the spray spot temperature also increases. As the temperature at the spray spot increases, previously deposited material softens, as shown in Figure 8, resulting in an increase in contact area when impacted by incoming particles, leading to the increase in bonding ratio shown in Figure 10. Improving the bonding between splats increases the strength of the bulk deposit. For the 5 kW case, the

temperature at the deposition spot is measured to be 455°C. At this temperature, the most drastic decrease in yield strength at the spray spot is expected, which leads to the strongest bonding between splats. Additionally, because the entire deposit is maintained at an elevated temperature and overaged, the overall hardness of the deposit decreases, as shown in Figure 6 and Figure 7. The combination of increased bonding ratio and decreased bulk hardness likely contribute to the high ductility seen in the 5 kW case.

The fracture surfaces of the tensile specimens are shown in Figure 13. In the TS-0kW-T case, presented in Figure 13a, the surface is smooth, exposing the exterior surfaces of the powder particles, indicating failure happened between splats. In the TS-3kW-H case, failure is still mostly between splats, but there is an increase in ductile dimples marked by white arrows in Figure 13b. These patches indicate areas of strong bonding, where localized strain occurred during the tensile test, causing the splat to tear at those locations, leading to dimples. The TS-5kW-H case, presented in Figure 13c, shows highly textured surfaces. Individual splats cannot be easily discerned as in the other cases. In this case, dominance is observed for dimple-like fracture in areas with strong bonding, while less significant unbonded regions can also be observed. Based on the tensile results, it is known that the inter-splat bond strength is high for the 5 kW case, as is the elongation along the splat boundaries. An increase in the bonding ratio and decrease in hardness allows the splats to deform significantly during tensile testing, forming the dimpled surfaces seen in Figure 13c.
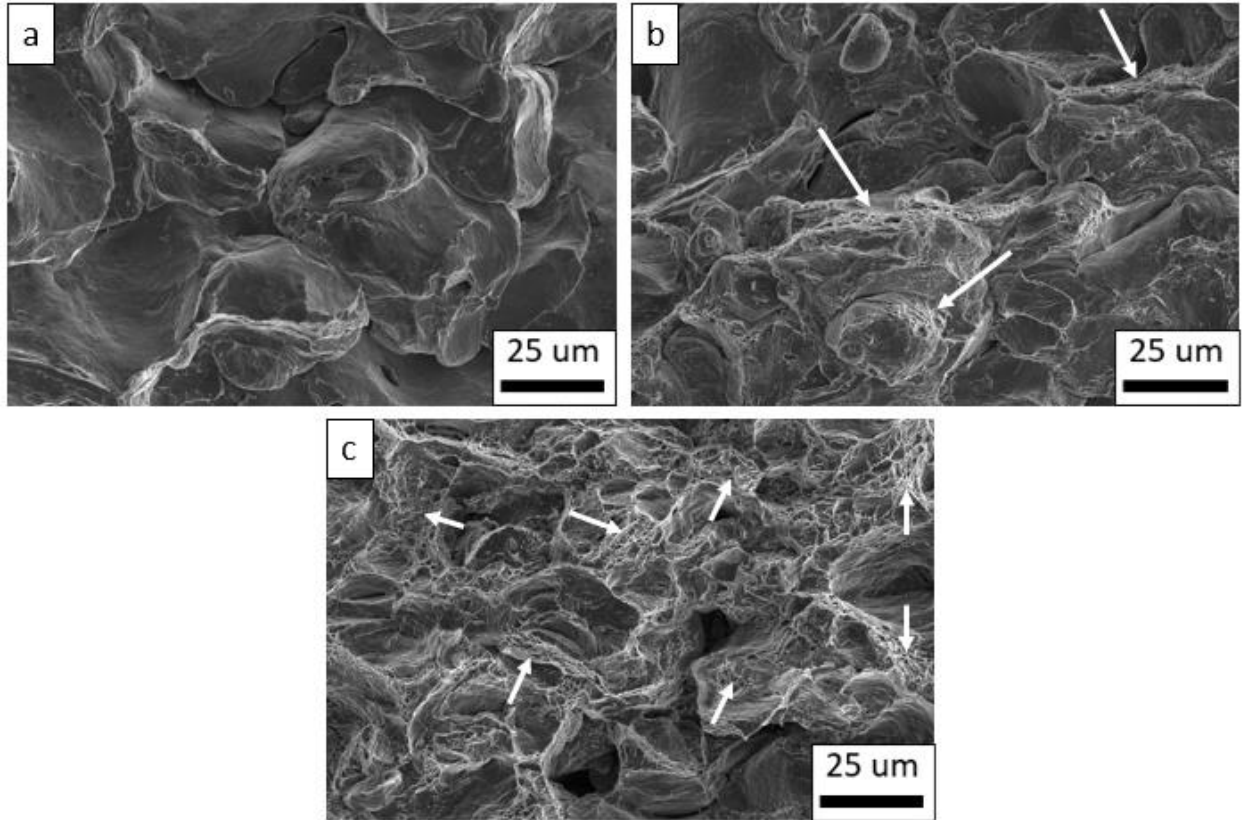
Figure 13. Fracture surfaces of (a) TS-0kW-T, (b) TS-3kW-H, and (c) TS-5kW-H. White arrows indicate ductile dimples.

4.5 Deposition efficiency (DE)

Deposition efficiency (DE) was calculated by measuring the weight of the deposit and comparing it to the weight of the powder that was fed during the deposition. Therefore, a higher DE correlates to less material waste and faster material throughput. The results are shown in Table 4. One DE measurement can be taken for each deposition, so the values shown are an average of the two tensile blocks sprayed for each condition. The control case (TS-0kW-T) has a DE of 38%, which increases to 63% for TS-3kW-H. The increase can be attributed to the decrease in yield strength at the spray spot modeled in Figure 8. When the spray surface is softened, there is a higher probability of particles adhering to it, leading to an increase in DE. The DE drops to 54% for the TS-5kW-H case. The decrease could be due to erosion. 5 kW causes significant softening of the deposit, this could allow the high-

pressure gas stream to partly erode the surface during deposition, causing a relative decrease in DE. Based on this data, material waste can be minimized with 3 kW of laser power.

Table 4. Deposition efficiencies (DEs) for different process conditions.

Sample	DE (%)
TS-0kW-T	38 ± 1
TS-0kW-I	39 ± 0.5
TS-0kW-H	54 ± 0.5
TS-1kW-H	58.5 ± 0.5
TS-3kW-H	63 ± 2
TS-5kW-H	54 ± 1

4.6 Residual Stress

Residual stress measurements were performed to show why the use of a hotplate beneath the substrate prevents delamination during LACS. The residual stress results are plotted in Figure 14. As expected, the case with no laser (RS-0kW-T) has a compressive residual stress, typical of CS deposits [39]. The use of 0.5 kW laser power (RS-0.5kW-T) causes the stresses to increase and have more variability. This is due to the high heat gradient caused by having a laser on the top surface of the deposit but no heating from below the substrate. The addition of the hotplate (RS-0.5kW-H) causes more uniformity in the residual stress. The results can explain the delamination of LACS samples prepared without heating from the hotplate. The large variation of residual stress, including a change from compressive to tensile stress, likely causes a curling in the samples that imposes a large normal stress in the interface, eventually leading to interface failure and delamination. The addition of the hotplate lessens the thermal gradient, lowering these residual stresses, and allowing the deposit to remain securely on the substrate.
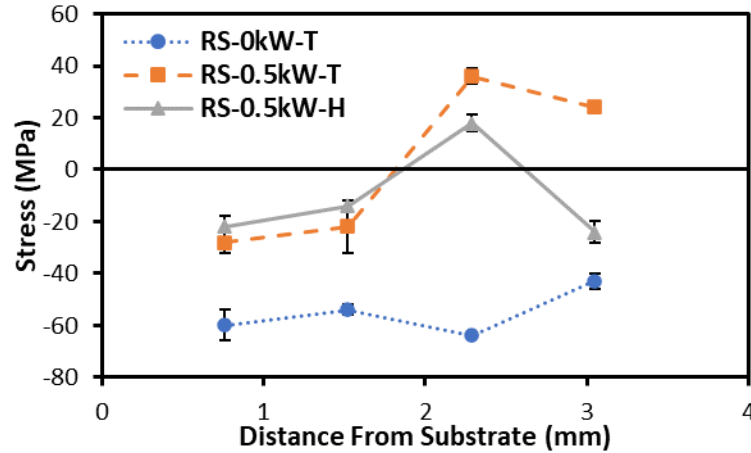
Figure 14. Residual stress measurements taken in the CS deposit in the longitudinal spray direction.

4.7 Fatigue performance and fractography

Results of the fatigue tests performed on F-3kW-H and F-5kW-H samples are shown in Figure 15. Wrought Al6061-T6 results are taken from the literature [12]. Fatigue performance was tested for F-3kW-H and F-5kW-H because the tensile results showed that 3 kW led to high strength and 5 kW led to high strength and ductility. Based on the results presented in Figure 15, the fatigue performance of the F-3kW-H and F-5kW-H samples are similar, implying that strength is the driving factor of fatigue performance for the LACS samples, and not ductility. Research shows that in the high-cycle fatigue (HCF) regime, tensile strength predominantly governs fatigue life [40]. With this understanding, it is normal to expect that the fatigue performance of the LACS samples to be lower than wrought Al6061-T6 samples. Samples manufactured without the laser were not tested for fatigue. The extremely low strength of the TS-0kW-T samples would not result in any significant fatigue performance.
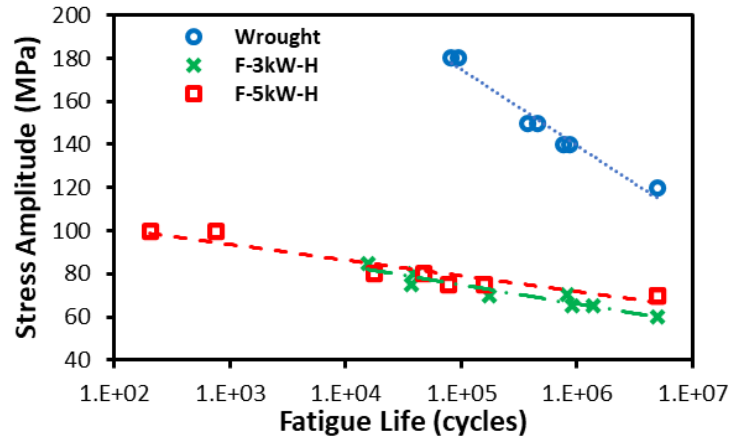
Figure 15. Fatigue performance of samples F-3kW-H and F-5kW-H compared to wrought Al6061-T6.

SEM fractography was performed on the fatigue samples, as shown in Figure 16. It can be seen that for all samples, crack initiation and propagation occur between splats, rather than the outer surface of the fatigue specimen. Multiple cracks initiated from the unbonded regions between the splats, as indicated by the beach marks on the fracture surfaces, highlighted with white arrows. In samples tested at relatively high stress amplitudes (Figure 16a and Figure 16c), a lower number of cracks were observed. Conversely, in samples tested at relatively low stress amplitudes (Figure 16b and Figure 16d), higher number beach marks were noticed, showing a longer crack growth region. These cracks propagated across a few particles before coalescing and transforming into unstable cracks, ultimately leading to rupture in the specimens.
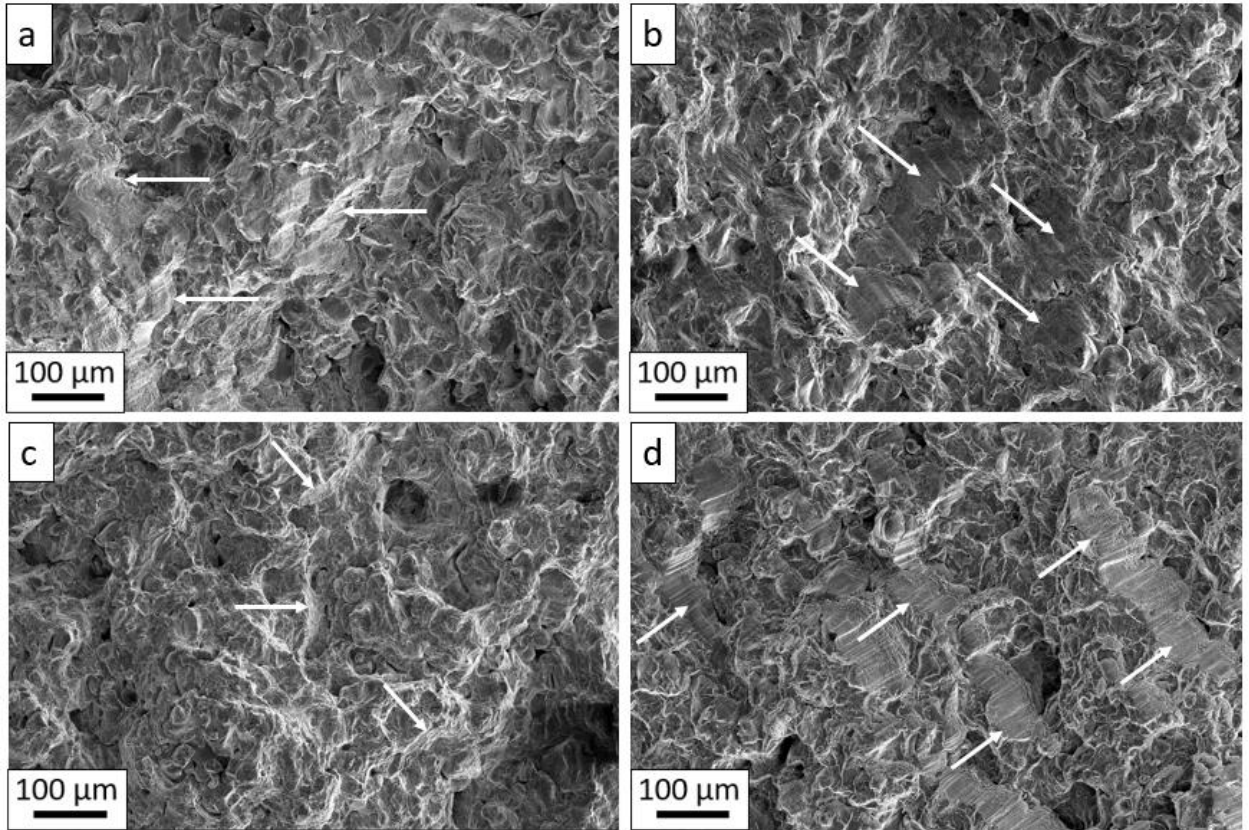
Figure 16. SEM images of fracture surface of specimens tested for fatigue. Images are of (a) F-3kW-H tested at 80 MPa, (b) F-3kW-H tested at 65 MPa, (c) F-5kW-H tested at 100 MPa, and (d) F-5kW-H tested at 75 MPa. Areas of crack propagation are identified with white arrows.

4.8   Adhesion Strength

The adhesion test results based on bond button testing are presented in Figure 17. Six samples were tested for each condition. Results show that an increase in laser power causes an increase in bond strength. The adhesion strength increases from 18.4 MPa to 76.8 MPa at 1 kW and 6 kW of laser power, respectively. The samples sprayed at 5 kW and 6 kW fail within the glue (i.e. glue failure), whereas the samples prepared by using lower laser powers failed at the coating (i.e. cohesive failure). Thus, the adhesion strength for the 5 kW and 6 kW samples is above 77 MPa, as the sprayed deposit itself did not fail. The minimum adhesion strength of the glue is reported by the manufacturer to be 68.9 MPa, which was surpassed in these tests. The increase in bond strength is likely due to the

improvement in bonding at the interface (i.e. between the splats and the substrate) and between splats that is facilitated by the addition of heat due to the laser.
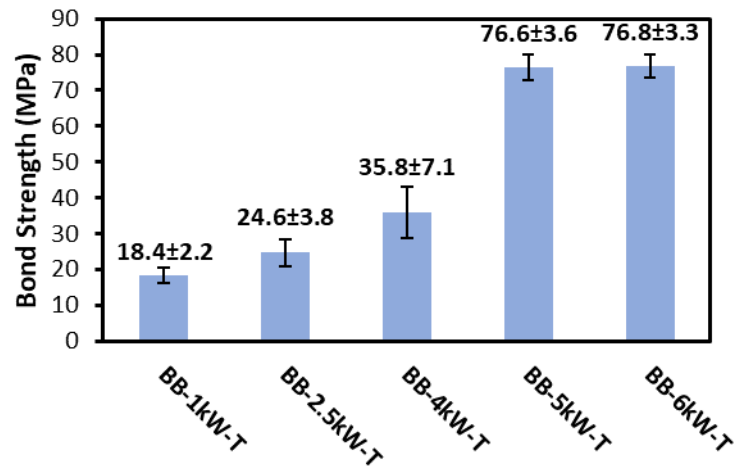

Figure 17. Average bond strength of Al6061 LACS deposits.

5 Conclusions and Future Work

5.1 Conclusions

For LACS of Al6061 in nitrogen, tensile testing showed a steady increase in strength from 34.3 MPa to 167.6 MPa as laser power is increased. There is a drastic increase in ductility at 5 kW, which improves from < 1% to 15.58%. Temperature data reveals that at 5 kW the deposition temperature surpasses the annealing temperature of Al6061, allowing for significant splat deformation and improved bonding. Metallographic analysis confirmed changes in hardness, disappearance of voids, consolidation of precipitates and recrystallization of grains. XRD shows that residual stresses induced by the laser can be mitigated by use of a hotplate, allowing the deposit to stay laminated to the substrate at high laser powers. Fatigue testing showed that the 3 kW and 5 kW cases exhibit similar fatigue performance, implying that fatigue life in the deposits is driven by tensile strength. There is an increase in adhesion strength from 18.4 MPa to 76.8 MPa as laser power is increased from 1 kW to 6 kW.

The laser can be used to control the metallurgical properties of the deposits. A higher laser power leads to more heat input, causing precipitation growth and grain consolidation, decreasing the overall hardness of the deposit. This creates the ability to achieve target hardness values by adjusting the laser power. At 0 kW of laser power the hardness of the deposit is approximately 80 HV and at 5 kW of laser power the hardness is 50 HV. The laser also creates changes at the splat boundaries. High laser powers soften deposited splats which allows incoming powder particles to form closer contact and therefore stronger bonds with neighboring splats. Strengthening the bonds between splats improves both the

strength and ductility of the bulk deposit. Mechanical properties of the LACS deposits are maximized at 5 kW, where strength is 167.6 MPa and ductility is 15.58%.

5.2 Future Work

Considering the success of LACS when used with Al6061, it is reasonable to expand this research to other material systems. Al6061 is a common cold sprayable aluminum alloy, primarily because of its moderate DE. It would be useful to spray other aluminum alloys in nitrogen, but it is less common due to their low DEs when compared to Al6061. This includes Al2024 and Al7075. These alloys are harder than Al6061 and therefore the particles show limited deformation upon impact during a CS process. This could be improved with LACS. Al2024 and Al7075 have similar softening temperatures and softening mechanisms as Al6061, namely recrystallization and precipitation growth. Therefore, the addition of the laser should lead to a softer deposition surface during CS deposition, allowing more particles to adhere and for DE to increase. In addition to an increase in DE, improvements in mechanical properties may be realized as they were in this work.

As the temperature demands of various mechanical systems advance, new material challenges are presented. Namely, nuclear power systems, turbines, and hypersonic vehicles sometimes operate at temperatures >1,000°C as they push the current limits of efficiency and speed. The problems created by these high operating temperatures may be solvable with CS and in some cases LACS. Metal coatings that can withstand high temperatures are known as refractory metals. Among these are Nb, Ta, and Ti. These materials can be deposited in helium but have inferior DE and mechanical properties when sprayed in nitrogen. Therefore, LACS may be a viable alternative to depositing refractory

metals using nitrogen. Refractory metals are fairly expensive when compared to more common powders such as aluminum and steel. Therefore, increases in DE when spraying refractory metals would lead to significant cost savings. The need for high temperature, durable coatings will more than likely increase in the coming decades, so finding a reliable method producing these coatings is critical.
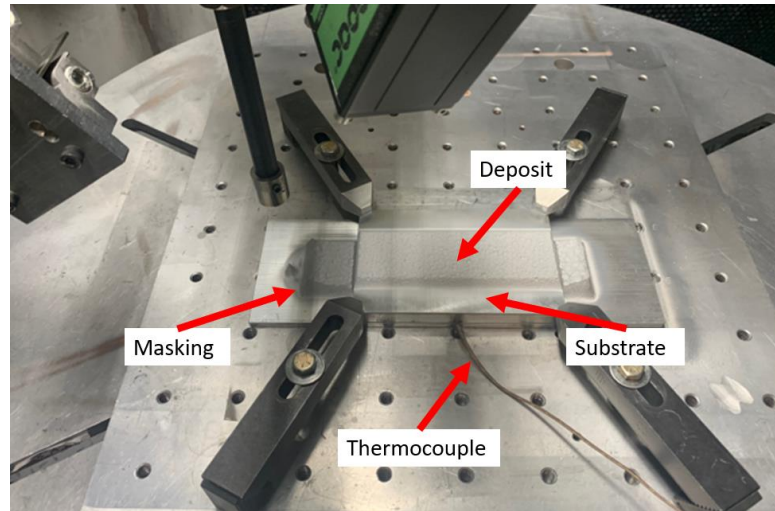
Appendix
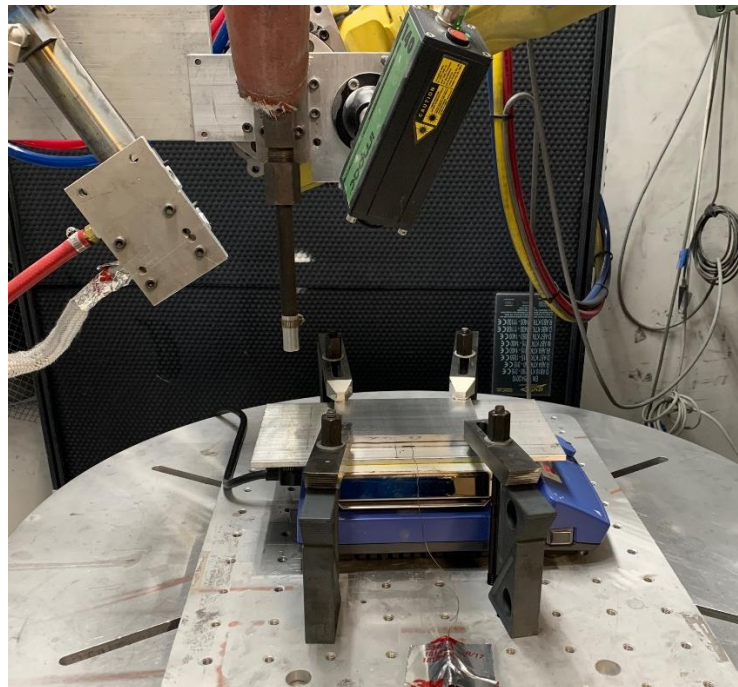

Figure 18. Al 6061 tensile block after a completed spray.

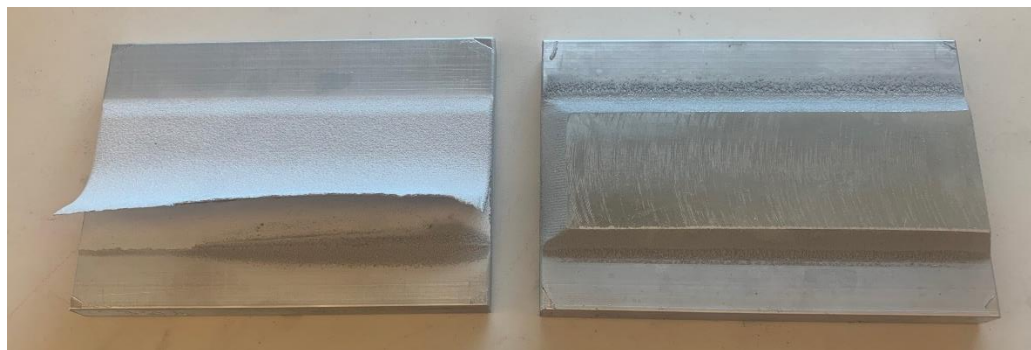Figure 19. Tensile block process setup including a hotplate.

Figure 20. Delaminated tensile block (left) and laminated tensile block after surface machining (right).
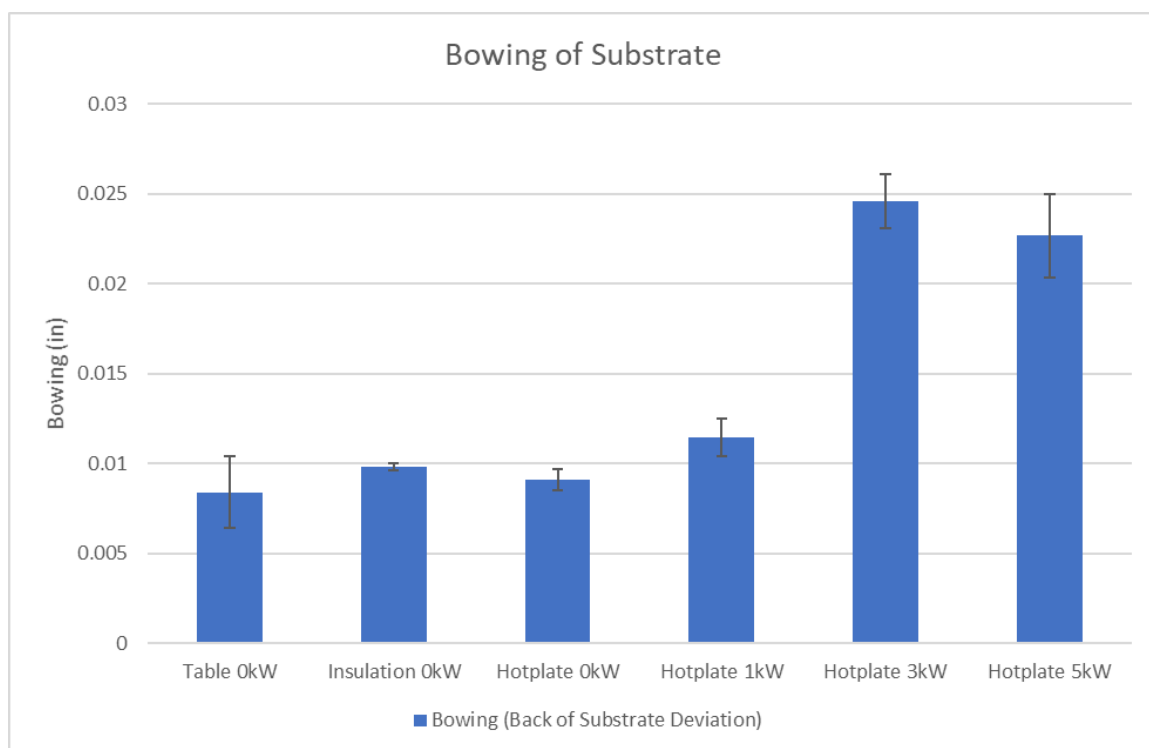

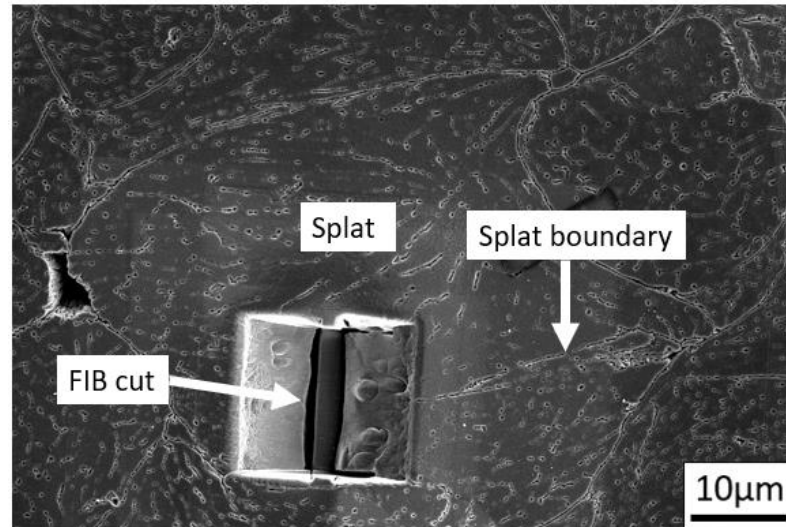Figure 21. Bowing of substrate for different deposition conditions of tensile blocks.

Figure 22. SEM of a splat after FIB milling to create a TEM sample. TEM samples were cut from the polar region of each splat.
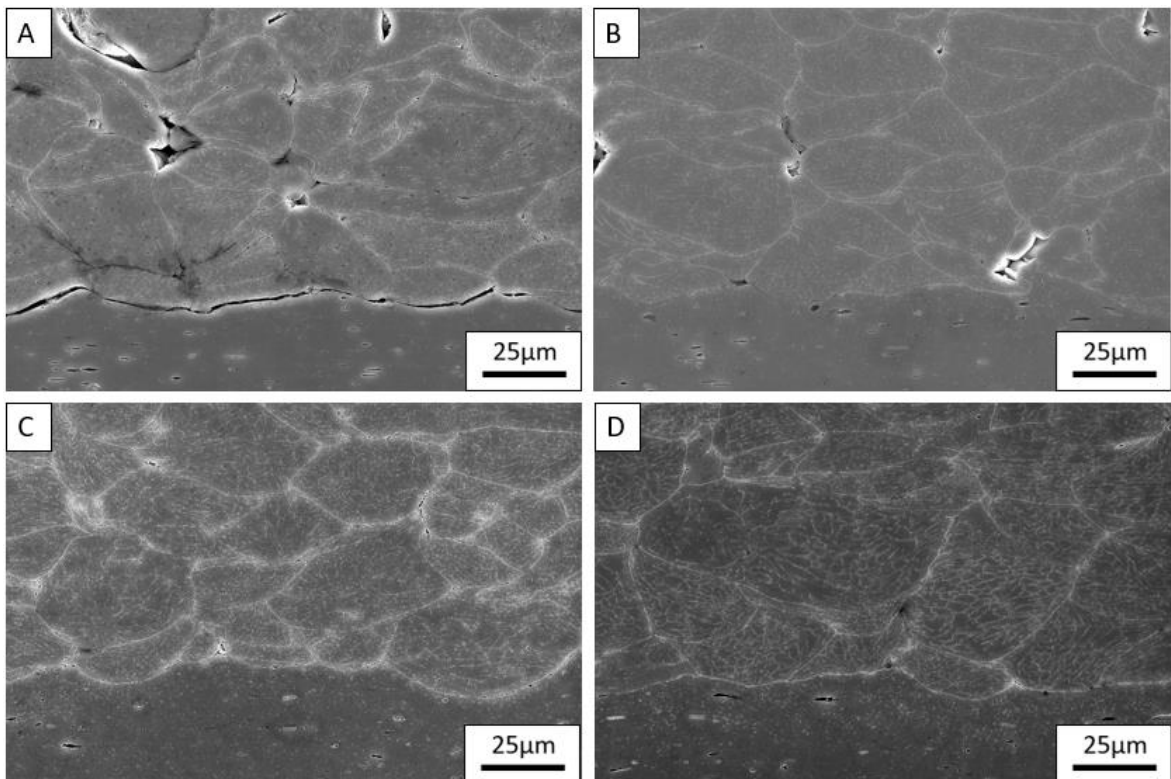

Figure 23. SEM of etched deposit taken at 2,500x magnification. Images are of samples (a) TS-0kW-T, (b) TS-0kW-H, (c) TS-3kW-H, and (d) TS-5kW-H.
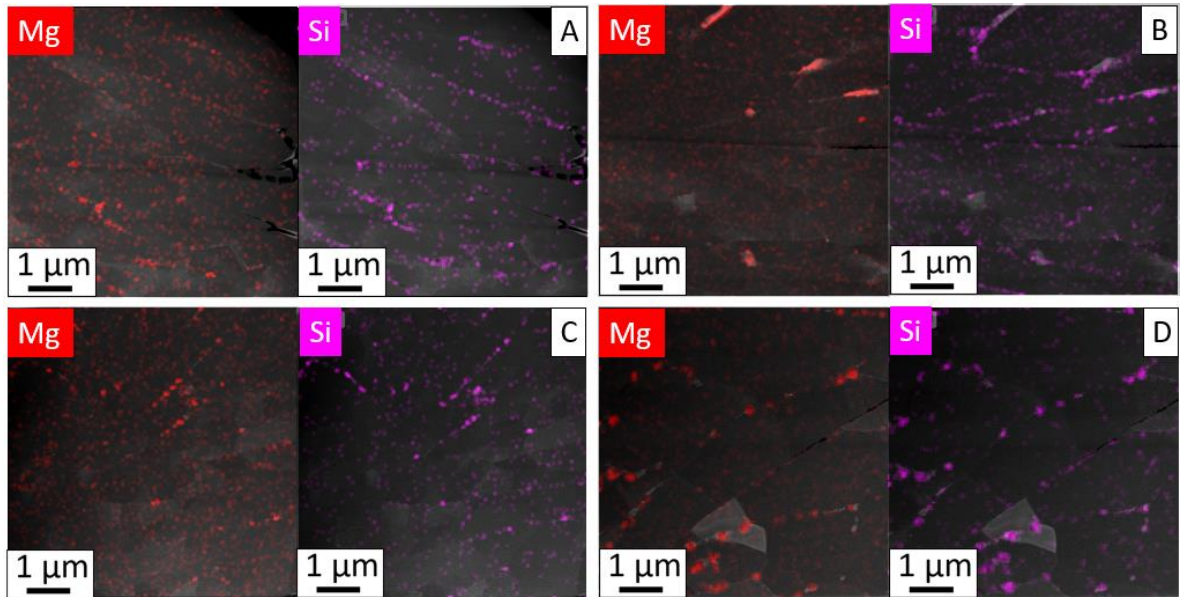
Figure 24. EDS images of Mg and Si overlayed with STEM images for (a) TS-0kW-T, (b) TS-0kW-H, (c) TS-3kW-H, and (d) TS-5kW-H.
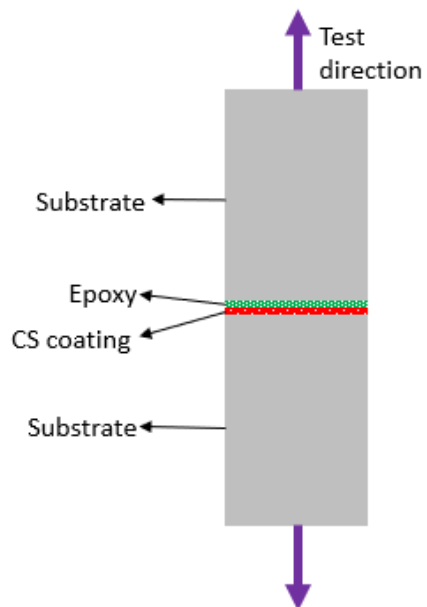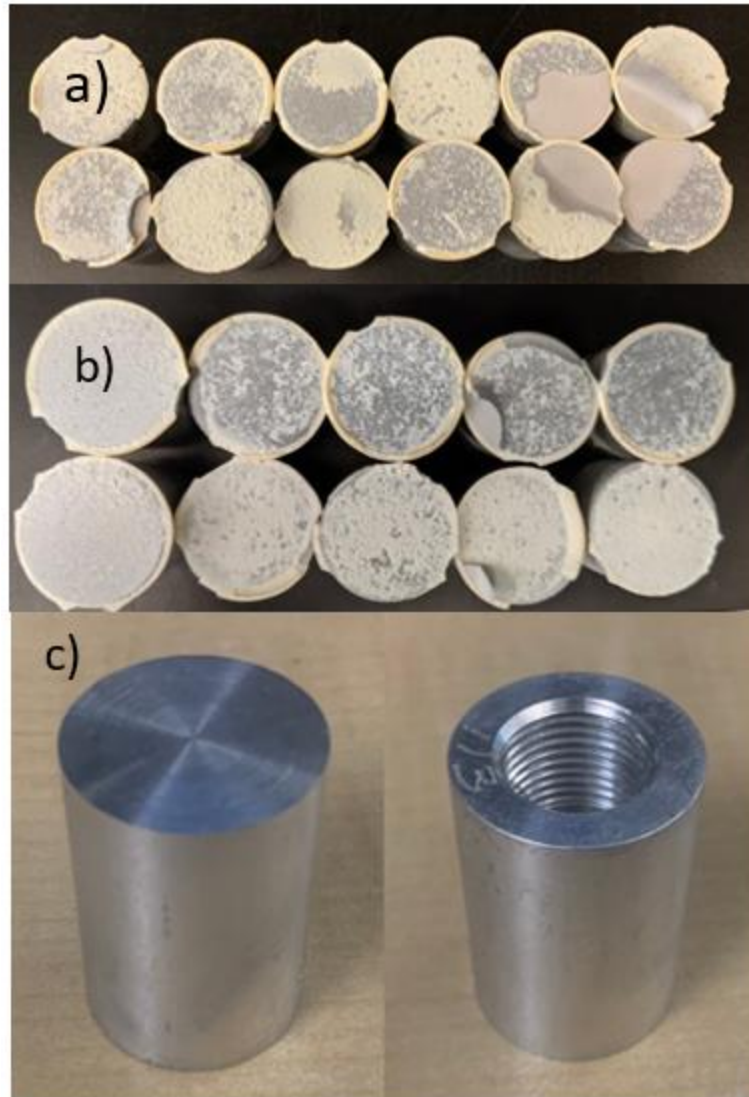

Figure 25. Bond button test schematic.

Figure 26. Pulled bond buttons showing flue failure for (a) 5 kW and (b) 6 kW samples. (c) Bond button specimen after machining and prior to cold spray deposition.
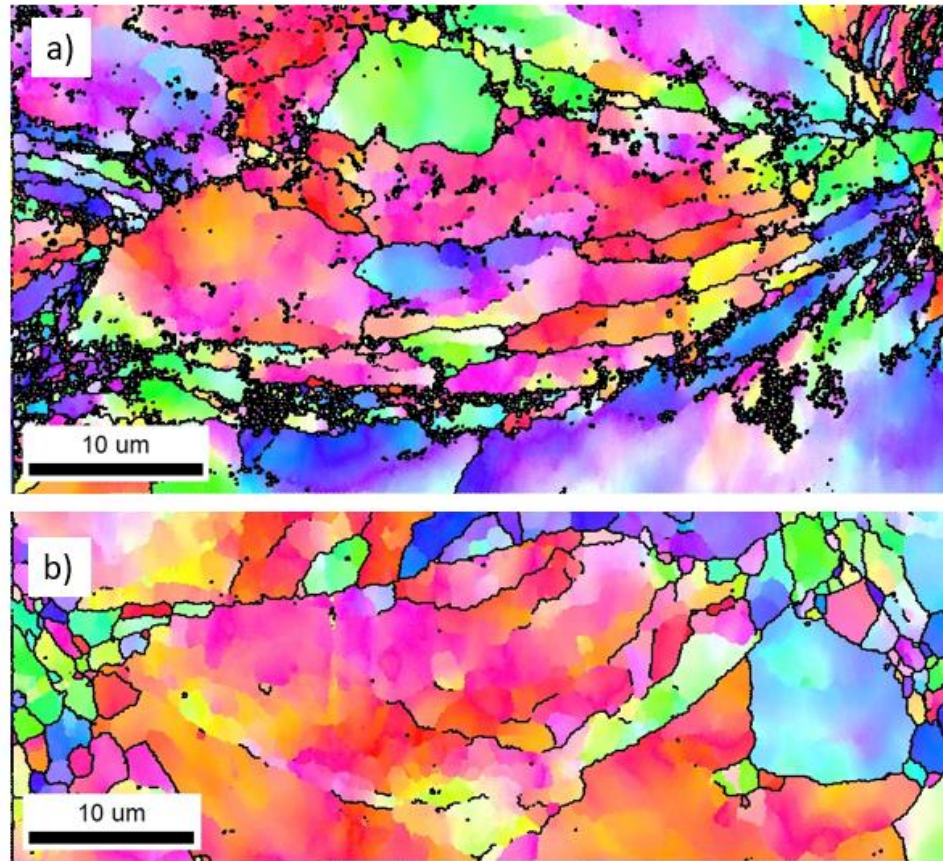
Figure 27. EBSD of singular splat for deposit created with (a) 1 kW and (b) 5 kW of laser power.

References

[1]   J. Villafuerte and SpringerLink, *Modern Cold Spray : Materials, Process, and Applications*, 1st 2015. ed. Cham: Springer International Publishing : Imprint: Springer (in English), 2015.

[2]   V. K. Champagne Jr, O. C. Ozdemir, A. Nardi, and SpringerLink, *Practical Cold Spray*, 1st 2021. ed. Cham: Springer International Publishing : Imprint: Springer (in English), 2021.

[3]   X. Qiu, L. Qi, J.-r. Tang, N. u. H. Tariq, J.-q. Wang, and T.-y. Xiong, "A viable approach to repair neutron shielding B4C/6061 Al composite sheets through cold spray and hot rolling co-treatment," *Journal of Materials Science & Technology,* vol. 106, pp. 173-182, 2022/04/20/ 2022, doi: https://doi.org/10.1016/j.jmst.2021.06.085.

[4]   S. A. Alidokht, P. Manimunda, P. Vo, S. Yue, and R. R. Chromik, "Cold spray deposition of a Ni-WC composite coating and its dry sliding wear behavior," *Surface and Coatings Technology,* vol. 308, pp. 424-434, 2016/12/25/ 2016, doi: https://doi.org/10.1016/j.surfcoat.2016.09.089.

[5]   N. Hutasoit, M. A. Javed, R. A. R. Rashid, S. Wade, and S. Palanisamy, "Effects of build orientation and heat treatment on microstructure, mechanical and corrosion properties of Al6061 aluminium parts built by cold spray additive manufacturing

process," *International Journal of Mechanical Sciences,* vol. 204, p. 106526, 2021/08/15/ 2021, doi: https://doi.org/10.1016/j.ijmecsci.2021.106526.

[6]   Y. Cormier, P. Dupuis, B. Jodoin, and A. Corbeil, "Mechanical Properties of Cold Gas Dynamic-Sprayed Near-Net-Shaped Fin Arrays," *Journal of Thermal Spray Technology,* vol. 24, no. 3, pp. 476-488, 2015/02/01 2015, doi: 10.1007/s11666-014-0203-1.

[7]   K. S. Al-Hamdani, J. W. Murray, T. Hussain, and A. T. Clare, "Heat-treatment and mechanical properties of cold-sprayed high strength Al alloys from satellited feedstocks," *Surface and Coatings Technology,* vol. 374, pp. 21-31, 2019/09/25/ 2019, doi: https://doi.org/10.1016/j.surfcoat.2019.05.043.

[8]   M. R. Rokni, C. A. Widener, O. C. Ozdemir, and G. A. Crawford, "Microstructure and mechanical properties of cold sprayed 6061 Al in As-sprayed and heat treated condition," *Surface and Coatings Technology,* vol. 309, pp. 641-650, 2017/01/15/ 2017, doi: https://doi.org/10.1016/j.surfcoat.2016.12.035.

[9]   W. C. Evans, X. Dan, A. Houshmand, S. Müftü, and T. Ando, "Microstructural Characterization of Aluminum 6061 Splats Cold Spray Deposited on Aluminum 6061-T6 Substrate," *Metallurgical and Materials Transactions A,* vol. 50, no. 8, pp. 3937-3948, 2019/08/01 2019, doi: 10.1007/s11661-019-05303-z.

[10]   C. Huang, A. List, J. Shen, B. Fu, S. Yin, T. Chen, B. Klusemann, F. Gärtner, and T. Klassen, "Tailoring powder strengths for enhanced quality of cold sprayed

Al6061 deposits," *Materials & Design,* vol. 215, p. 110494, 2022/03/01/ 2022, doi: https://doi.org/10.1016/j.matdes.2022.110494.

[11]   A. Sabard and T. Hussain, "Inter-particle bonding in cold spray deposition of a gas-atomised and a solution heat-treated Al 6061 powder," *Journal of Materials Science,* vol. 54, no. 18, pp. 12061-12078, 2019/09/01 2019, doi: 10.1007/s10853-019-03736-w.

[12]   A. Nourian and S. Müftü, "Effect of substrate surface finish and particle velocity on fatigue performance of cold spray coated A6061 aluminum alloy," *Surface and Coatings Technology,* vol. 444, p. 128676, 2022/08/25/ 2022, doi: https://doi.org/10.1016/j.surfcoat.2022.128676.

[13]   A. G. Gavras, D. A. Lados, V. K. Champagne, and R. J. Warren, "Effects of processing on microstructure evolution and fatigue crack growth mechanisms in cold-spray 6061 aluminum alloy," *International Journal of Fatigue,* vol. 110, pp. 49-62, 2018/05/01/ 2018, doi: https://doi.org/10.1016/j.ijfatigue.2018.01.006.

[14]   S. E. Julien, A. Nourian-Avval, W. Liang, T. Schwartz, O. C. Ozdemir, and S. Müftü, "Bulk fracture anisotropy in Cold-Sprayed Al 6061 deposits," *Engineering Fracture Mechanics,* vol. 263, p. 108301, 2022/03/15/ 2022, doi: https://doi.org/10.1016/j.engfracmech.2022.108301.

[15]   B. Aldwell, E. Kelly, R. Wall, A. Amaldi, G. E. O'Donnell, and R. Lupoi, "Machinability of Al 6061 Deposited with Cold Spray Additive Manufacturing,"

Journal of Thermal Spray Technology, vol. 26, no. 7, pp. 1573-1584, 2017/10/01 2017, doi: 10.1007/s11666-017-0586-x.

[16]	Y.-K. Wei, X.-T. Luo, X. Chu, G.-S. Huang, and C.-J. Li, "Solid-state additive manufacturing high performance aluminum alloy 6061 enabled by an in-situ micro-forging assisted cold spray," *Materials Science and Engineering: A,* vol. 776, p. 139024, 2020/03/03/ 2020, doi: https://doi.org/10.1016/j.msea.2020.139024.

[17]	T. J. Flanagan, B. A. Bedard, A. M. Dongare, H. D. Brody, A. Nardi, V. K. Champagne, M. Aindow, and S.-W. Lee, "Mechanical properties of supersonic-impacted Al6061 powder particles," *Scripta Materialia,* vol. 171, pp. 52-56, 2019/10/01/ 2019, doi: https://doi.org/10.1016/j.scriptamat.2019.06.024.

[18]	H. Koivuluoto, J. Larjo, D. Marini, G. Pulci, and F. Marra, "Cold-Sprayed Al6061 Coatings: Online Spray Monitoring and Influence of Process Parameters on Coating Properties," *Coatings,* vol. 10, no. 4, p. 348, 2020. [Online]. Available: https://www.mdpi.com/2079-6412/10/4/348.

[19]	A. Nourian, C. Beamer, and S. Muftu, "Effects of post-deposition processing on static and cyclic performance of cold sprayed 6061 aluminum alloy," *Additive Manufacturing,* vol. 88, p. 104246, 2024/05/25/ 2024, doi: https://doi.org/10.1016/j.addma.2024.104246.

[20]	O. C. Ozdemir, C. A. Widener, D. Helfritch, and F. Delfanian, "Estimating the Effect of Helium and Nitrogen Mixing on Deposition Efficiency in Cold Spray,"

Journal of Thermal Spray Technology, vol. 25, no. 4, pp. 660-671, 2016/04/01 2016, doi: 10.1007/s11666-016-0394-8.

[21]   M. Bray, A. Cockburn, and W. O'Neill, "The Laser-assisted Cold Spray process and deposit characterisation," *Surface and Coatings Technology,* vol. 203, no. 19, pp.   2851-2857,   2009/06/25/   2009,   doi: https://doi.org/10.1016/j.surfcoat.2009.02.135.

[22]   N. H. Tariq, L. Gyansah, X. Qiu, H. Du, J. Q. Wang, B. Feng, D. S. Yan, and T. Y. Xiong, "Thermo-mechanical post-treatment: A strategic approach to improve microstructure and mechanical properties of cold spray additively manufactured composites," *Materials & Design,* vol. 156, pp. 287-299, 2018/10/15/ 2018, doi: https://doi.org/10.1016/j.matdes.2018.06.062.

[23]   D. J. Barton, V. S. Bhattiprolu, G. B. Thompson, and L. N. Brewer, "Laser assisted cold spray of AISI 4340 steel," *Surface and Coatings Technology,* vol. 400, p. 126218, 2020/10/25/ 2020, doi: https://doi.org/10.1016/j.surfcoat.2020.126218.

[24]   D. C. Dumitras, *Nd YAG Laser*. IntechOpen, 2012.

[25]   W. A. Story, D. J. Barton, B. C. Hornbuckle, K. A. Darling, G. B. Thompson, and L. N. Brewer, "Laser assisted cold spray of Fe–Ni–Zr oxide dispersion strengthened steel,"   *Materialia,*   vol.   3,   pp.   239-242,   2018/11/01/   2018,   doi: https://doi.org/10.1016/j.mtla.2018.08.028.

[26]   A. Birt, V. Champagne Jr, R. Jr, and D. Apelian, "Statistically Guided Development of Laser-Assisted Cold Spray for Microstructural Control of Ti-6Al-4V,"

Metallurgical and Materials Transactions A, vol. 48, 02/06 2017, doi: 10.1007/s11661-017-3970-8.

[27] M. Kulmala and P. Vuoristo, "Influence of process conditions in laser-assisted low-pressure cold spraying," *Surface and Coatings Technology,* vol. 202, no. 18, pp. 4503-4508, 2008/06/15/ 2008, doi: https://doi.org/10.1016/j.surfcoat.2008.04.034.

[28] E. O. Olakanmi, M. Tlotleng, C. Meacock, S. Pityana, and M. Doyoyo, "Deposition Mechanism and Microstructure of Laser-Assisted Cold-Sprayed (LACS) Al-12 wt.%Si Coatings: Effects of Laser Power," *JOM,* vol. 65, no. 6, pp. 776-783, 2013/06/01 2013, doi: 10.1007/s11837-013-0611-6.

[29] J.-G. Legoux, B. Guerreiro, D. Poirier, and J. D. Giallonardo, "Laser Assisted Cold Spray for Improved Adhesion of Soft Materials to Hard Substrates—Case Study for Copper Coatings on Steel," presented at the ITSC2021, 2021. [Online]. Available: https://doi.org/10.31399/asm.cp.itsc2021p0596.

[30] H. Koivuluoto, A. Milanti, G. Bolelli, J. Latokartano, F. Marra, G. Pulci, J. Vihinen, L. Lusvarghi, and P. Vuoristo, "Structures and Properties of Laser-Assisted Cold-Sprayed Aluminum Coatings," (in English), *Materials Science Forum,* vol. 879, pp. 984-989, Nov 2016

2020-09-22 2016, doi: http://dx.doi.org/10.4028/www.scientific.net/MSF.879.984.

[31] *ASTM Standard E8/E8M*, A. International, West Conshohocken, PA, 2021 1924. [Online]. Available: www.astm.org

[32]   *ASTM Standard E466*, A. International, West Conshohocken, PA, 2021 1972. [Online]. Available: www.astm.org

[33]   *Standard Test Method for Adhesion or Cohesion Strength of Thermal Spray Coatings*, A. International, 100 Barr Harbor Drive, PO Box C700, West Conshohocken, PA 19428-2959. United States, 2021.

[34]   G. E. Totten, A. S. M. I. H. Committee, and A. S. M. H. T. Society, *ASM handbook* (ASM handbook volume 4E). Materials Park, OH: ASM International (in English), 2016.

[35]   E. Lin, Q. Chen, O. C. Ozdemir, V. K. Champagne, and S. Müftü, "Effects of Interface Bonding on the Residual Stresses in Cold-Sprayed Al-6061: A Numerical Investigation," *Journal of Thermal Spray Technology,* vol. 28, no. 3, pp. 472-483, 2019/02/01 2019, doi: 10.1007/s11666-019-00827-7.

[36]   Q. Chen, A. Alizadeh, W. Xie, X. Wang, V. Champagne, A. Gouldstone, J.-H. Lee, and S. Müftü, "High-Strain-Rate Material Behavior and Adiabatic Material Instability in Impact of Micron-Scale Al-6061 Particles," *Journal of Thermal Spray Technology,* vol. 27, no. 4, pp. 641-653, 2018/04/01 2018, doi: 10.1007/s11666-018-0712-4.

[37]   W. Sun, A. W.-Y. Tan, K. Wu, S. Yin, X. Yang, I. Marinescu, and E. Liu, "Post-Process Treatments on Supersonic Cold Sprayed Coatings: A Review," *Coatings,* vol. 10, no. 2, p. 123, 2020. [Online]. Available: https://www.mdpi.com/2079-6412/10/2/123.

[38]   W.-Y. Li, C.-J. Li, and H. Liao, "Effect of annealing treatment on the microstructure and properties of cold-sprayed Cu coating," *Journal of Thermal Spray Technology,* vol. 15, no. 2, pp. 206-211, 2006/06/01 2006, doi: 10.1361/105996306X108066.

[39]   V. Luzin, K. Spencer, and M. X. Zhang, "Residual stress and thermo-mechanical properties of cold spray metal coatings," *Acta Materialia,* vol. 59, no. 3, pp. 1259-1270, 2011/02/01/ 2011, doi: https://doi.org/10.1016/j.actamat.2010.10.058.

[40]   S. S. Manson and M. H. Hirschberg, "The role of ductility, tensile strength and fracture toughness in fatigue," *Journal of the Franklin Institute,* vol. 290, no. 6, pp. 539-548, 1970/12/01/ 1970, doi: https://doi.org/10.1016/0016-0032(70)90236-X.